Article

Current Biology

Fertilization-dependent phloem end gate regulates seed size

Graphical abstract

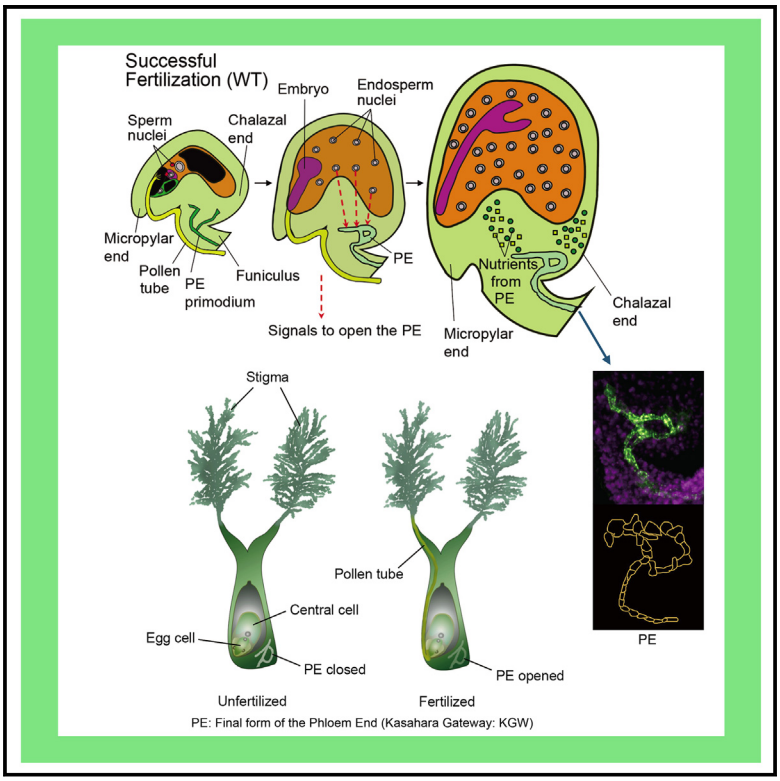

Highlights

- A brand-new seed nutrition system by a novel plant "gate" tissue was identified
- The gate is open when a plant fertilizes but stays closed when fertilization fails
- The structure of the gate is identified as the final form of the phloem end in plants
- Both *Arabidopsis* and rice seeds: the seed size can be modified by AtBG_ppap

Authors

Xiaoyan Liu, Kohdai P. Nakajima, Prakash Babu Adhikari, ..., Kent J. Bradford, Michitaka Notaguchi, Ryushiro D. Kasahara

Correspondence

notaguchi.michitaka.4k@kyoto-u.ac.jp (M.N.), kasahara.ryushiro.s2@f.mail.nagoya-u.ac.jp (R.D.K.)

In brief

Liu et al. identify a fertilization-dependent "gate," a new plant tissue located at the ovule, which is open when a plant fertilizes and stays closed when a plant fails fertilization, having an essential function in controlling seed formation by using a wise mechanism in plants, which leads to a great potential for seed-focused plant breeding.

Liu et al., 2025, Current Biology *35*, 2049–2063
May 5, 2025
https://doi.org/10.1016/j.cub.2025.03.033

CellPress

Current Biology

CellPress
OPEN ACCESS

Article

Fertilization-dependent phloem end gate regulates seed size

Xiaoyan Liu,[1,2,12] Kohdai P. Nakajima,[3,12] Prakash Babu Adhikari,[4] Xiaoyan Wu,[1,2] Shaowei Zhu,[1,2] Kentaro Okada,[4] Tomoko Kagenishi,[5] Ken-ichi Kurotani,[4] Takashi Ishida,[6,7] Masayoshi Nakamura,[8] Yoshikatsu Sato,[8] Yaichi Kawakatsu,[4] Liyang Xie,[1,2] Chen Huang,[1,2] Jiale He,[1,2] Ken Yokawa,[5] Shinichiro Sawa,[6,7] Tetsuya Higashiyama,[9] Kent J. Bradford,[10] Michitaka Notaguchi,[4,11,*] and Ryushiro D. Kasahara[4,13,*]

[1]School of Life Sciences, Fujian Agriculture and Forestry University, Fuzhou, Fujian 350002, China
[2]FAFU-UCR Joint Center and Fujian Provincial Key Laboratory of Haixia Applied Plant Systems Biology, Haixia Institute of Science and Technology, Fujian Agriculture and Forestry University, Fuzhou, Fujian 350002, China
[3]Department of Biology, Technion-Institute of Technology, Haifa 320000, Israel
[4]Bioscience and Biotechnology Center, Nagoya University, Furo-cho, Chikusa, Nagoya, Aichi 464-8601, Japan
[5]Faculty of Engineering, Kitami Institute of Technology, 165 Koen-cho, Kitami, Hokkaido 090-8507, Japan
[6]Graduate School of Science & Technology, Kumamoto University, 2-39-1 Kurokami, Chuo-ku, Kumamoto 860-8555, Japan
[7]International Research Organization for Advanced Science and Technology (IROAST), Kumamoto University, 2-39-1 Kurokami, Chuo-ku, Kumamoto 860-8555, Japan
[8]Institute of Transformative Bio-Molecules (WPI-ITbM), Nagoya University, Furo-chou, Chikusa-ku, Nagoya, Aichi 464-8601, Japan
[9]Department of Biological Sciences, Graduate School of Science, The University of Tokyo, 7-3-1 Hongo, Bunkyo-ku, Tokyo 113-0033, Japan
[10]Department of Plant Sciences, Seed Biotechnology Center, University of California, Davis, Davis, CA 95616, USA
[11]Department of Botany, Graduate School of Science, Kyoto University, Kitashirakawa Oiwake-cho, Kyoto 606-8502, Japan
[12]These authors contributed equally
[13]Lead contact
*Correspondence: notaguchi.michitaka.4k@kyoto-u.ac.jp (M.N.), kasahara.ryushiro.s2@f.mail.nagoya-u.ac.jp (R.D.K.)
https://doi.org/10.1016/j.cub.2025.03.033

SUMMARY

Seed formation is essential for plant propagation and food production. We present a novel mechanism for the regulation of seed size by a newly identified "gate" at the chalazal end of the ovule regulating nutrient transport into the developing seed. This gate is blocked by callose deposition in unfertilized mature ovules (closed state), but the callose is removed after central cell fertilization, allowing nutrient transport into the seed (open state). However, if fertilization fails, callose deposition persists, preventing transportation of nutrients from the funiculus. A mutant in an ovule-expressed β-1,3-glucanase gene (*AtBG_ppap*) showed incomplete callose degradation after fertilization and produced smaller seeds, apparently due to its partially closed state. By contrast, an *AtBG_ppap* overexpression line produced larger seeds due to continuous callose degradation, fully opening the gate for nutrient transport into the seed. The mechanism was also identified in rice, indicating that it potentially could be applied widely to angiosperms to increase seed size.

INTRODUCTION

Seed size is one of the critical traits in plant breeding and crop yields. Although several genes required for normal seed size have been identified,[1–5] the mechanisms underlying the direct effects of most genes on the phenotype are yet to be investigated at the molecular level. A rare example of known molecular mechanisms is the amino acid (aa) transporter UmamiT, and plants with defective UmamiT produce smaller seeds than wild-type (WT) plants because the mutant cannot transport aa into developing seeds.[6] Therefore, nutrient supply contributes to determining seed size, which offers the potential for enhancing crop seed enlargement. Nutrients supplied by maternal tissues are essential for embryo formation and development in animals and plants. In flowering plants, the transmitting tract and funiculus fully develop before fertilization as a unique nutritional support system for the seed. However, the molecular mechanism by which plants supply nutrients from the transmitting tract to developing seeds after fertilization is not fully understood. Although fertilization by pollen nuclei is necessary for seed formation,[7–10] with the exception of apomixis,[11–13] whether fertilization is required to initiate or continue the nutrient transport required for normal seed formation remains to be investigated in detail. Similarly, studies that have identified nutritional transporters in the ovule reported that molecular approaches were required to explain how fertilization triggers ovule nutrition to support seed formation.[6,14–17] Mutation of the *Arabidopsis generative cell-specific 1* (*gcs1*) or *hapless 2* (*hap2*) gene results in pollen grains that contain fertilization-defective sperm cells (*GCS1*/*HAP2*).[18–20] Although seed expansion was partially initiated by the release of *gcs1* pollen tube contents into the ovule, further development was arrested and resulted in a unique pollen tube-dependent ovule enlargement morphology (POEM).[21–25] These POEM results indicate that a fertilization-dependent regulatory mechanism is required to support subsequent seed development.

In this study, we demonstrate a new plant nutritional regulatory mechanism that is governed by callose deposition/degradation specifically in a unique structure at the chalazal end of the ovule where the phloem from the mother plant that supports nutrient transport into the ovule terminates. Phloem unloading occurs here, and nutrients are exported into the apoplast to be absorbed by the developing embryo and endosperm.[26,27] Callose deposition in this phloem end (PE) structure increases if fertilization fails, but this callose is degraded if the ovule is successfully fertilized. Expression of the *AtBG_ppap* gene (TAIR ID: At5g42100), previously shown to encode a putative plasmodesmata-associated β-1,3-glucanase (a callose-degrading enzyme),[28] is upregulated only after successful fertilization, and its expression is correlated with both callose degradation and increased seed size. A defect in *AtBG_ppap* (*Atbg_ppap* mutant) leads to an increase in callose deposition, interfering with nutrient supply to the developing seeds and negatively affecting their size. By contrast, overexpression of *AtBG_ppap* (*OEAtBG_ppap*) increases callose degradation and seed size due to unimpeded nutrient flow to the developing seed following callose degradation. Central cell fertilization (leading to endosperm development) but not egg cell fertilization alone activates callose degradation and initiation of nutrient transport. The PE structure is also present in rice seeds, and seed size can be enhanced by overexpressing a *PPAP* gene, indicating that modification of callose deposition in this structure can potentially be applied widely across angiosperms to produce larger seeds.

RESULTS

Callose deposition follows failure of fertilization

As callose accumulation in the leaf phloem reduces axillary bud growth,[29] it might also significantly affect seed formation and development. We therefore stained ovules of emasculated and pollinated flowers over several days. We observed significant callose deposition around the chalazal end of the phloem (cyan ellipses in Figure 1) after aniline blue staining[30] at 2–4 days after emasculation (DAE) in no pollen tube (NPT) (unfertilized) ovules (Figures 1A–1C). The signal was not observed at 2 DAE, which is equivalent to 1 day after pollination (DAP, Figure 1A), but gradually increased at $\geq$3 DAE (Figures 1B and 1C). In WT (fertilized) ovules, the signal was observed at 1 DAP (Figure 1D) but became weaker at 2 and 3 DAP (Figures 1E and 1F), indicating that callose deposition was transiently promoted at 1 DAP (=2 DAE) and then diminished thereafter. As mentioned earlier, the *gcs1* mutant does not produce seeds because its sperm cells are defective and cannot fertilize egg or central cells. When WT flowers were pollinated with *gcs1* pollen, which are unable to effect fertilization, the signal remained consistently intense, even at $\geq$2 DAP (Figures 1G–1I). Signal intensities were observed every 4 h after fertilization (WT) or fertilization failure (*gcs1*) (Figure S1). At 24 h after pollination (HAP) in the WT, the signal intensity began to decrease and was reduced 10-fold by 48 HAP. By contrast, after pollination with *gcs1* pollen, the signal consistently intensified between 24 and 48 HAP.

The phenotypic differences in callose content among WT, NPT, and *gcs1* ovules depended on whether fertilization occurred. If fertilization was successful, callose did not accumulate at the chalazal end, but callose deposition continued if fertilization failed. The amount of callose deposition was lower in the NPT ovules (Figures 1A–1C) compared with the *gcs1* ovules (Figures 1G–1I), suggesting that the NPT ovules remained receptive to pollen tubes and therefore continued to receive some nutrients from mother tissue. Such nutrient flow is apparently cut off after failure of fertilization in the case of *gcs1* ovules. To further investigate this phenomenon, three-dimensional images of WT (Figures 1J–1N; Video S1) and *gcs1* ovules (Figures 1O–1S; Video S1) were captured at 2 DAP. In WT ovules, the central region of callose deposition was degraded, showing a ring-shaped signal, whereas *gcs1* ovules displayed a saturated signal. However, both exhibited similar circular structures. These results indicate that callose deposition persists if ovule fertilization fails, whereas if ovules are fertilized, the deposits are degraded. An additional region in the ovule with callose deposition was observed above the ring-shaped structure. However, since the discrepancy was more evident for the lower region among the differentially fertilized ovules, we focused our study on it.

As the callose deposition area overlapped with the phloem unloading region,[17] we hypothesized that callose deposition regulates the nutrition supply during seed formation. To test this hypothesis, the cells of both WT and *gcs1* ovules at 3 DAP were stained with aniline blue and observed using the *RPS5Apro::tdTomato-LTI6b* membrane marker line.[31] In the WT, the callose signal was weak (Figure 1T), and the early developing seed showed normal growth with intact membrane structures (Figure 1U). However, in *gcs1*, the callose signal remained intense (Figure 1V), and the membrane marker showed the signs of degrading cells (Figure 1W). Although the main body of the ovule developed abnormally, the funiculus below the ovule developed normally (Figure 1X). The intensification of the callose plug coincided with the blockage at the end of the funiculus. After fertilization, the callose decreases, and nutrients are delivered from the placenta to the ovule to support seed development, with the PE functioning as a "gateway" to transport nutrients from the maternal parent to the seed.

Identification of callose-degrading enzyme genes encoding β-1,3-glucanase

Previously described expression patterns of callose-degrading enzyme genes[21] were explored in greater detail (Figure S2A). Genes encoding the callose-degrading enzyme β-1,3-glucanase are part of a large gene family in *Arabidopsis*. A homology search based on the aa sequence of a typical gene from this family (*β-1,3-glucanase 1*) identified 49 genes in the *Arabidopsis* genome. The expression profiles of all genes were compared, and 47 transcripts derived from the expression of 36 genes were detected during the first 48 h of fertilization in WT. Of the 47 transcripts, 14 were highly expressed at 48 h post-fertilization, and 11 had peak expression at 48 h. Among them, eight transcripts were not upregulated in *gcs1* ovules, suggesting that these genes are associated with callose degradation deficiency in *gcs1* (Figure S2B). Among these, genes encoding putative plasmodesmata-associated proteins (*AtBG_ppap*; At5g42100),[28] *β-1,3-glucanase 1* (*BG1*; At3g57270), and At4g29360 were annotated as encoding callose degradation enzymes. Since fold-change of *AtBG_ppap* expression was the most significant in the post-fertilization time course, we focused further on this gene. *AtBG_ppap* was highly expressed in the flower cluster and ovules at 2 DAP but

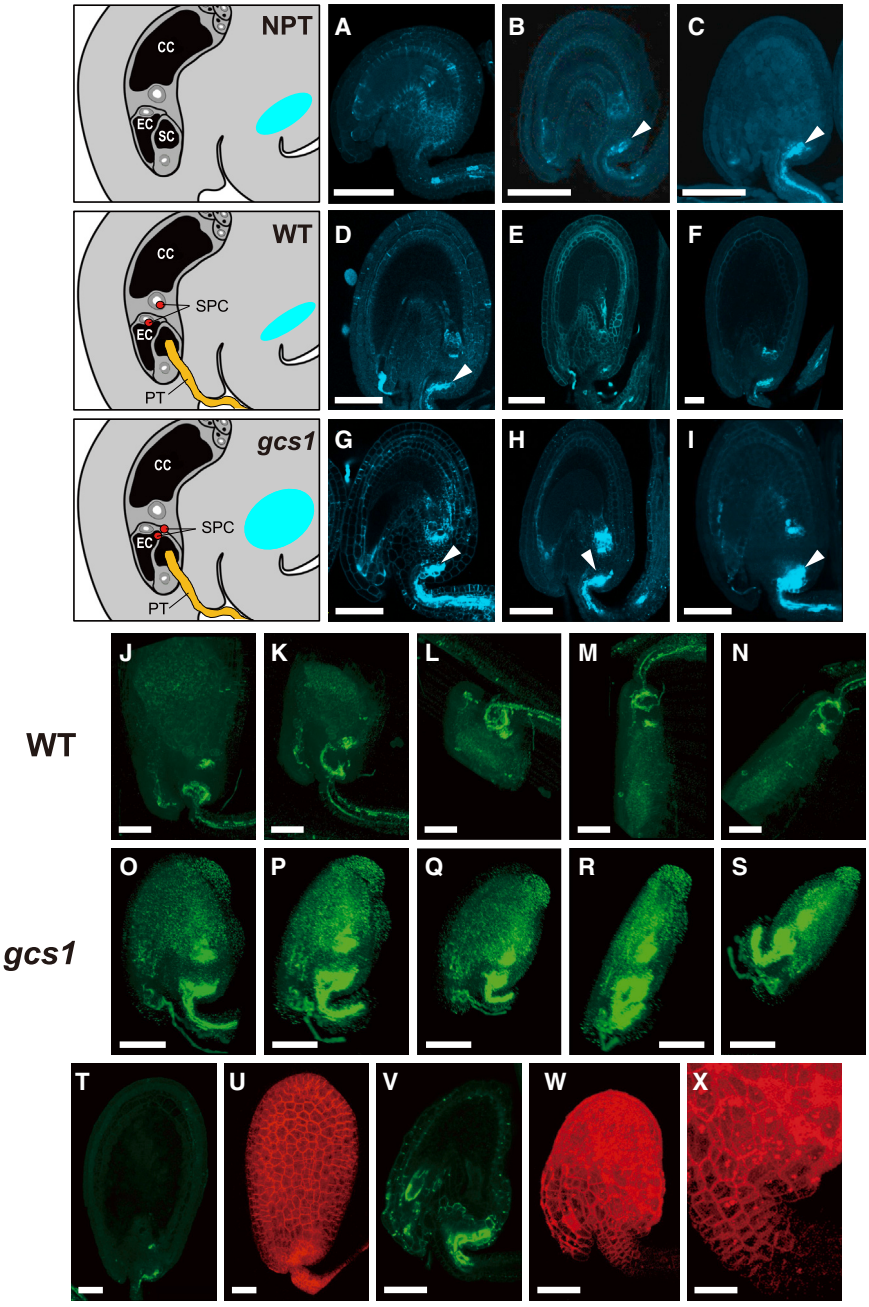

Figure 1. Discovery of the callose deposition phenomenon

(A–C) Aniline blue staining of ovules with no pollen tubes (NPTs) at 2 days after emasculation (DAE) (A), 3 DAE (B), and 4 DAE (C).

(D–F) WT ovules at 1 day after pollination (DAP) (equivalent to 2 DAE) (D), 2 DAP (=3 DAE) (E), and 3 DAP (=4 DAE) (F).

(G–I) *gcs1* ovules at 1 DAP (G), 2 DAP (H), and 3 DAP (I). Cyan ovals in the diagrams at left indicate the position and intensity of the aniline blue-stained regions.

(J–S) Rotated images of callose deposition in the WT and *gcs1* ovules (Video S1). (J–N) Aniline blue staining of WT ovules. Low-intensity circular callose deposits were detected at the chalazal end of the ovule. (O–S) Aniline blue staining of the *gcs1* ovules. Intensive callose deposition was observed at the chalazal end of the ovule.

(T–W) Aniline blue staining (T) and *RPS5Apro::tdTomato-LTI6b* expression (U) in WT at 3 DAP. Aniline blue staining (V) and *RPS5Apro::tdTomato-LTI6b* expression (W) in *gcs1* 3 DAP. (X) High magnification of the funicular/chalazal region in (W). Although the main body of the *gcs1* ovule developed abnormally, the funiculus below the PE developed normally. Scale bars: 50 μm (A–I), 20 μm (J–S), and 50 μm (T–X).

CC, central cell; EC, egg cell; SC, synergid cell; SPC, sperm cell; PT, pollen tube.

See also Figure S1 and Video S1.

was expressed at a low level in the cauline leaf and rosette leaf (Figure S2C). This *AtBG_ppap* gene consists of two exons, one of which is 1,209 bp and the other is 69 bp, bridged by one intron (433 bp) (Figure S3A). CRISPR technology was applied to create an *Atbg_ppap* mutant harboring a mutation site at 102 bps from ATG, resulting in a frameshift mutation (Figure S3B). While the aa sequence of the AtBG_ppap protein contains 425 aa, the Atbg_ppap mutant protein has an early termination codon that would code for a truncated protein of 87 aa (Figure S3C).

Identification of the final form of the PE

The detailed structure of the PE remains unclear, although a premature state has been described.[17] The final form of the phloem was visualized using the phloem marker *MtSEO2::GFP-ER*.[32,33] At 1 DAE, the PE exhibited a branched structure with two phloem tubes (Figure 2A; Video S2), similar to that described previously.[17] However, at 2 DAP (equivalent to 3 DAE), the shape was further modified to a circular structure (Figure 2B; Video S3), indicating the final form of the PE in the ovule. As the PE was identified and its position was close to that of callose deposition, the spatial relationship between the two was further investigated.

The phenotype of *Atbg_ppap* mutant was investigated using transcriptomic data (Figure S2) and aniline blue staining. Faint callose deposition, highlighted by a yellow line, was observed in the WT (Figure 2C; Video S4), unlike the intense deposition in *gcs1* (Figure 2D). However, although the intensity of the callose deposition is moderate, *Atbg_ppap* ovules showed persistent callose deposition, even after fertilization (Figure 2E; Video S5). The structure of the callose deposition (Figures 2E and sketched in 2F; Video S5) was identical to the final form of the PE (Figure 2B; Video S3). We also observed the bright signal for xylem cells (Figures 2C and 2E). We also investigated the PE in *Oryza sativa* as a representative monocot. The pistils were harvested and dissected to prepare sections for aniline blue staining. In the unfertilized sections of *osgcs1*,[34] high-intensity signals of callose deposition from the circular PE structure were clearly

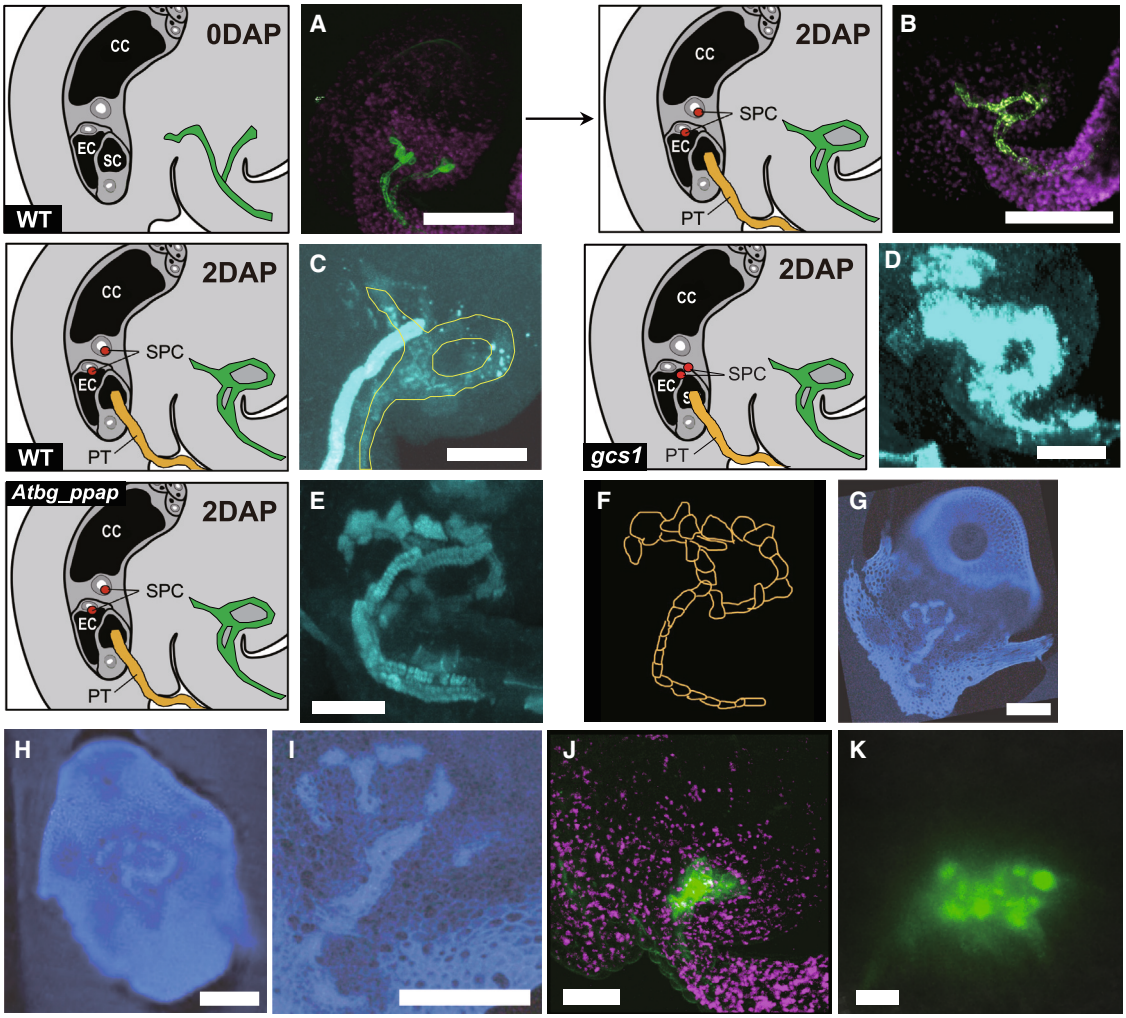

Figure 2. Detailed structure of the multi-functional PE of the ovule

(A and B) *MtSEO2::GFP-ER* (phloem marker; Video S2) at 0 DAP indicating branched phloem tubes (green staining) (A) and at 2 DAP indicating the final form of the PE (Video S3) (B).

(C–F) Detailed structures of callose deposition parts in WT (C, outlined by yellow shape; Video S4), *gcs1* (D), and *Atbg_ppap* (E; Video S5), with a diagram of the PE structure (F). The structure with the brightest signal in (C) and similar structure in (E) represent xylem.

(G–K) Ovule sections were obtained from fertilized and unfertilized ovules from Nipponbare rice. Aniline blue staining for an unfertilized ovule (G) and a fertilized ovule at 2 DAP (H). The signal from the PE in (G) was more intense than in (H). Magnified PE region (I) from (G). The PE structure in rice (G–I) is similar to that of *Arabidospsis* (E and F). *AtSWEET10-GFP* was expressed at the PE (J and K) in WT at 2 DAP, exclusively in the upper half of the PE (F). The purple color in (A), (B), and (J) represents autofluorescence.

Scale bars: 50 μm (A and B), 20 μm (C–E, J, and K), and 100 μm (G–I).

CC, central cell; EC, egg cell; SC, synergid cell; DAP, days after pollination; SPC, sperm cell; PT, pollen tube.

See also Figures S2–S4 and Videos S2, S3, S4, and S5.

observed (Figure 2G). Sections from fertilized ovaries also showed the PE; however, the callose deposition signals were weaker (Figure 2H), suggesting that callose deposition and degradation are dependent on fertilization in rice, as observed in *Arabidopsis*. The magnified image (Figure 2I) shows that the structure and callose deposition patterns were almost identical to those of *Arabidopsis* (Figures 2E and sketched in 2F). These results suggest that post-fertilization removal of callose by AtBG_ppap at the PE is associated with nutrient transport through the phloem to the PE region of the ovule in both *Arabidopsis* and rice.

Sucrose unloading in the ovule likely occurs via sucrose transporters. Previous studies[21] have shown upregulation of sugars will eventually be exported transporter (SWEET) sucrose transporters[35,36] in the WT ovules after fertilization (Figure S4). Among the 17 *SWEET* genes in *Arabidopsis*, three genes, *SWEET1*, *7*, and *10*, were upregulated at 48 HAP in the WT but were down-regulated or remained nearly flat at 24–48 h in *gcs1* (Figure S4A). Phylogenetic analysis of the 17 *SWEET* genes revealed that *SWEET1*, *7*, and *10* did not form a specific clade (Figures S4B and S4C). Notably, in the WT, *SWEET10* promoter-driven GFP expression was observed exclusively at the gate (Figure 2J)

and was limited to the upper part (Figure 2K) of the structure (Figure 2F). Together with previous observations that phosphate and aa transporters (i.e., UmamiT) are also located at the gate in the ovule,[6,14–17] the PE identified in this study has at least two structural functions: a site for nutrient unloading in the ovule and a gateway exhibiting callose deposition/degradation.

Callose deposition blocks unloading in the PE in the absence of fertilization

To test whether callose deposition can block nutrient influx from the placenta to the ovule, experiments were designed to observe the influx of substances from the phloem into the ovule using carboxyfluorescein (CF) diacetate (CFDA).[37,38] Live-cell imaging using the Ikebana method (Figure S5) showed that the CF symplastic tracer was transported to the ovule's main body through the gate in WT ovules (Figure 3A, arrowheads; Video S6). However, it was not transported through the gate in *gcs1* ovules (Figure 3B, arrowheads; Video S7), suggesting that the gate halted nutrient flow from the funiculus in response to fertilization failure. In *Atbg_ppap* ovules, CF was barely observed in the main body (Figure 3C arrowheads; Video S8), indicating that the gate partially impeded the nutrient flow despite successful fertilization. When CF was observed in *AtBG_ppap* overexpression (*OEAtBG_ppap*) lines with the 35S promoter, the signal was detected in the main body but was weaker than that observed in the WT and *Atbg_ppap* at the gate portion (Figure 3D; Video S9), suggesting that CF is somewhat impeded at the PE structure in WT ovules and takes time to be dispersed, although amounts of callose are relatively low. However, *OEAtBG_PPAP* plants have much lower amounts of the callose, and the CF is not impeded at the PE, as no signal could be detected in the funiculus (Figure 3D), suggesting that it is promptly supplied to the main body of the ovule and then dispersed quickly. Figure 3E illustrates the structure of the *Atbg_ppap* chalazal end stained by aniline blue with mature PE cells outlined in yellow (Figure 3F) and peripheral cells outlined in white (Figure 3G).

Central cell fertilization activates opening of the gate

Although our findings suggest that fertilization is required to degrade callose and open the gate for nutrients, the type of fertilization (egg or central cell) that initiates callose degradation remains unclear. *gcs1* is useful for testing morphological changes in the ovule during double fertilization failure; however, it is not applicable in the case of single fertilization, where one sperm cell fertilizes either the egg cell or the central cell, but the other sperm cell does not. Hence, *kokopelli* (*kpl*) mutant pollen,[39] which induces double fertilization at a 28% frequency, egg cell single fertilization at 23%, central cell single fertilization at 18%, and no fertilization (POEM) at 24%, was used for further assessment. A single fertilization event in either the egg or the central cells was confirmed by aniline blue staining of each ovule at 2 DAP. Callose was degraded in double-fertilized and central cell single-fertilized ovules (Figures 4A and 4B). However, the signal was intense in egg cell single-fertilized ovules (Figure 4C), suggesting that central cell fertilization is required for callose degradation.

Based on our hypothesis that callose deposition could block nutrient flow, subsequent experiments were conducted to demonstrate whether the deposition-blocked substance influx into the ovule was affected by the type of fertilization. Again using CFDA to trace sucrose influx,[37,38] we also examined the background cell membranes using *RPS5Apro::tdTomato-LTI6b* marker and used *WOX2p::H2B-GFP* + *WOX2p::LTI-tdTomato*[40] double markers for embryos and the *AGL62::GFP*[41] marker for endosperm. An intense CF signal was observed above the PE of double-fertilized or central cell single-fertilized ovules (Figures 4D–4G or Figures 4H–4K arrowheads). However, this was not observed above the PE of egg cell single-fertilized ovules (Figures 4L–4O), indicating that nutrient transport did not occur if central cell fertilization failed (Figure 4P). Essentially identical results were obtained with esculin (Figure S6), indicating sucrose transport.[36,42,43] An intense esculin signal was observed above the PE of the double- or central cell single-fertilized ovules (Figures S6A–S6C or Figures S6D–S6F). However, this was not observed above the PE of the egg cell single-fertilized ovules (Figures S6G–S6I) compared with that seen in WT ovules (Figure S6J), nor in POEM ovules (Figure S6K), indicating that sucrose transport did not occur when the central cell fertilization of the ovule failed. These results showed that transport of sucrose and other substances occurred only after central cell fertilization (Figure S6L), accompanied by callose degradation.

Atbg_ppap produces smaller seeds, and *OEAtBG_ppap* produces larger seeds

To further investigate this nutrient-blocking effect, the sizes of mature seeds were measured. Compared with the WT seeds (Figure 5A), the seeds produced by the *Atbg_ppap* mutant were 8.4% smaller (Figures 5B and 5C). A complementation test for *Atbg_ppap* with the WT *AtBG_ppap* gene was performed and resulted in seed size similar to that of WT (Figure S7A). To investigate whether *Atbg_ppap* affected other ovule phenotypes, the ovule areas and numbers were examined, and no significant differences were found between WT and *Atbg_ppap* lines (Figures S7B and S7C). Similarly, the heights of the plants were not significantly different (Figure S7D). These results indicated that the *Atbg_ppap* mutation specifically affected the seed size phenotype. By contrast, *OEAtBG_ppap* produced seeds that were 16.5% larger than the WT (Figures 5D–5F). To investigate whether *OEAtBG_ppap* (OE) was highly expressed in the ovules before and after fertilization, the expression patterns of WT and OE were compared using quantitative reverse-transcription PCR (Figure S8A). OE was highly expressed at 0 and 2 DAP, compared with the WT. WT and OE plants showed no significant differences in the sizes and numbers of ovules per pistil (Figures S8B and S8C) or in plant height or cotyledon, rosette leaf, and cauline leaf sizes (Figures S8D–S8G). However, OE seeds were larger than WT seeds from 1 to 3 DAP (Figure S8H). These results indicated that the *OEAtBG_ppap* line exclusively affected the enlargement of the seed size in *Arabidopsis*. As a proof of concept, we also investigated whether rice seed size would be increased in a line overexpressing the *Arabidopsis*-derived *AtBG_ppap* gene driven by the 35S promoter. In this case, the *OEPPAP* seeds (right in Figure 5G) were 9% larger than the Nipponbare seeds (left in Figure 5G and data in Figure 5H).

These results strongly suggest that the incomplete callose degradation in the *Atbg_ppap* mutant interfered with the nutrient

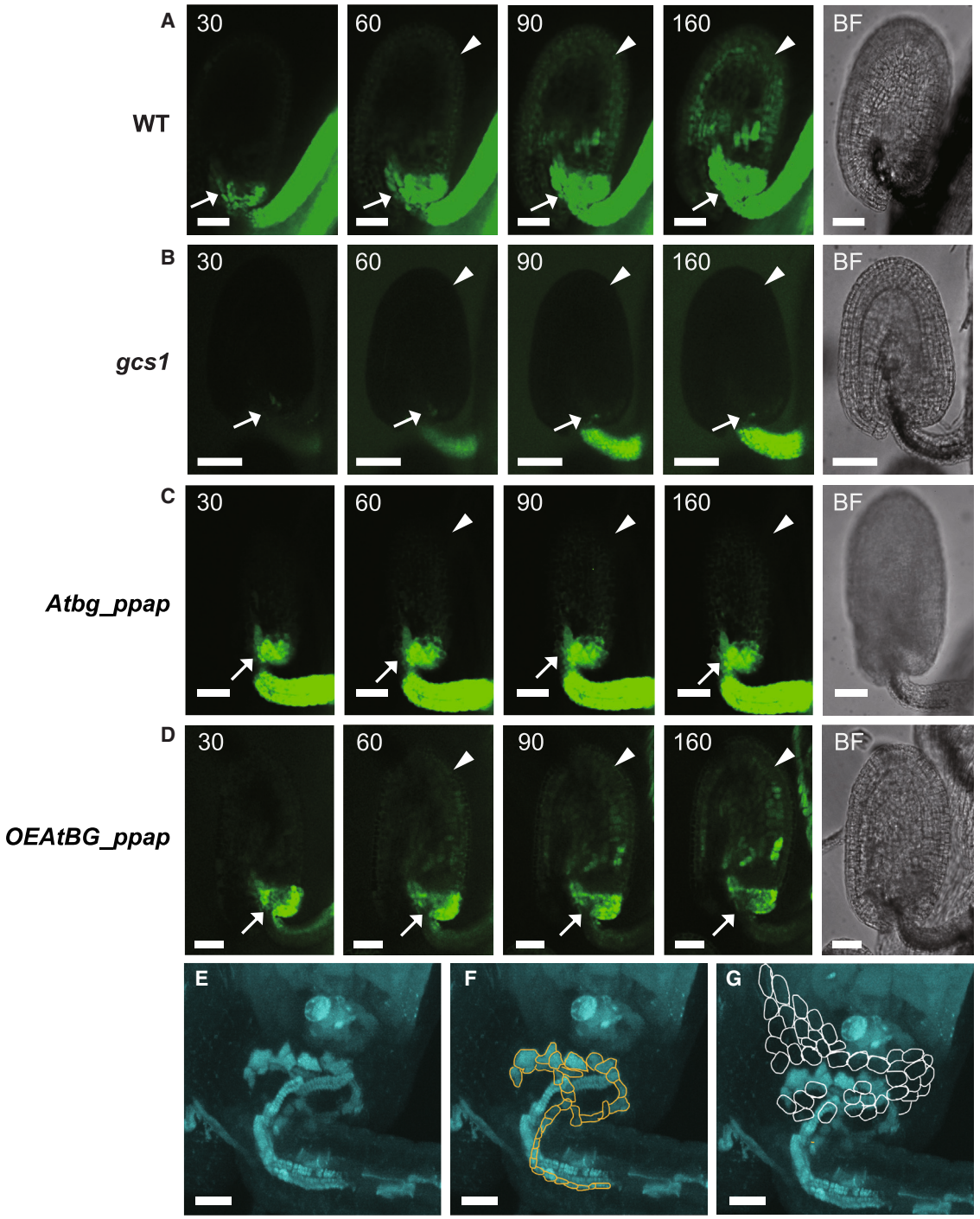

Figure 3. Nutrient flow is regulated by fertilization and AtBG_ppap

(A–D) Live-cell imaging of CF dye tracer flow in bright field and in videos at 30, 60, 90, and 160 min after the absorption of CF in WT (A, Video S6), in *gcs1* (B, Video S7), in *Atbg_ppap* (C, Video S8), and in *OEAtBG_ppap* lines (D, Video S9). Arrows indicate the position of callose deposition. Arrowheads: main body of the ovule.

(E–G) The structure of the WT chalazal end stained for callose (E) with mature PE cells outlined in yellow (F) and peripheral cells outlined in white (G). These were sketched based on (A) and Video S6.

Scale bars: 50 μm (A–D) and 20 μm (E–G).

See also Figures S2, S3, S5, and S6 and Videos S6, S7, S8, and S9.

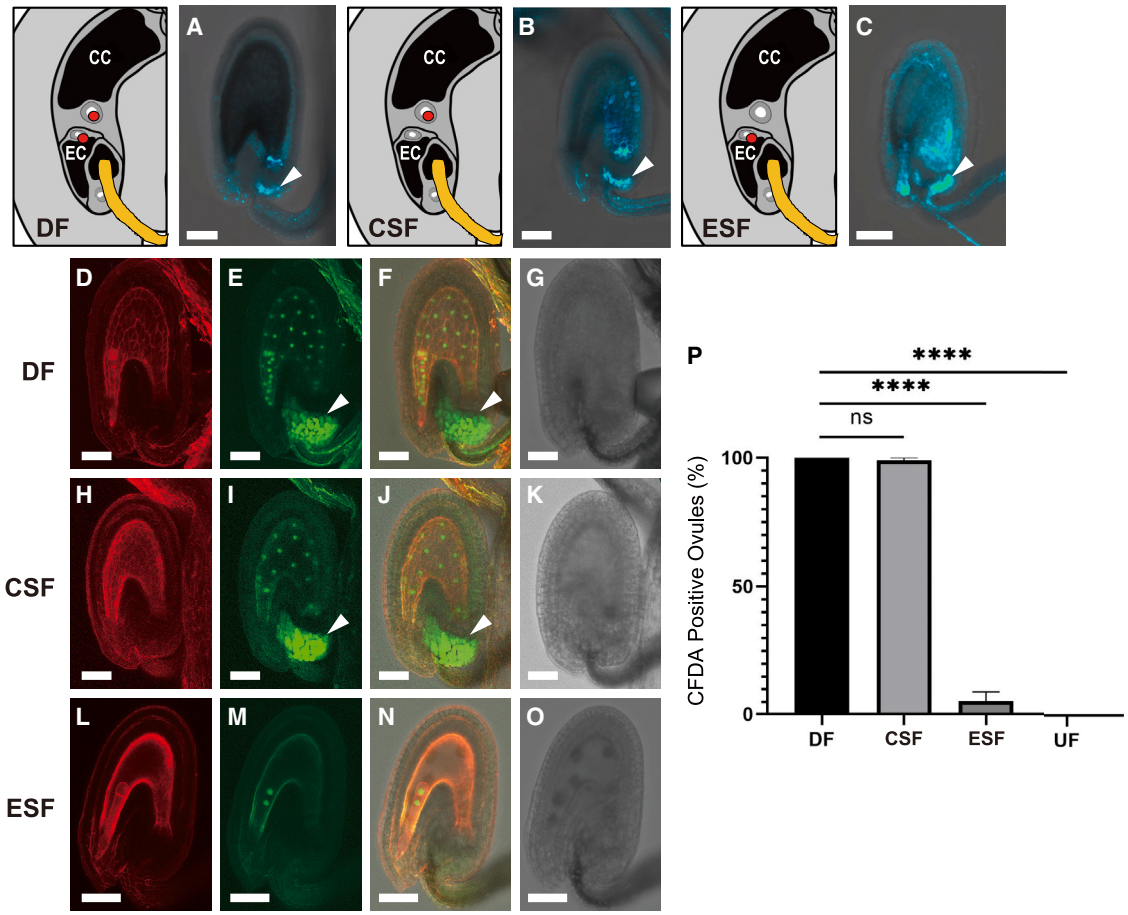

Figure 4. Central cell fertilization activates callose degradation and nutrient flow

(A–C) Aniline blue staining at 2 DAP after double fertilization (DF) (A), central cell (CC) single fertilization (CSF) (B), and egg cell (EC) single fertilization (ESF) (C). (D–O) Arrowheads indicate callose deposition. Expression in DF (D–G), CSF (H–K), and ESF (L–O) ovules of the *WOX2p::H2B-GFP* + *WOX2p::LTI-tdTomato* double marker (D, H, and L) and *AGL62::GFP* (E, I, and M) along with merged (F, J, and N) and bright-field (G, K, and O) images. Arrowheads indicate CF dye tracer signals (E, F, I, and J).

(P) Percentage of carboxyfluorescein (CF) symplastic dye tracer-positive ovules (P) for DF: 100% ± 0% (n = 403 ovules); CSF: 98.5% ± 0.9% (n = 68 ovules); ESF: 5.8% ± 3.3% (n = 120 ovules); and unfertilized (UF): 0% ± 0% (n = 54 ovules). Dunnett's multiple comparison test was used to assess the significance of differences. ****$p < 0.0001$. ns, no significance. Scale bars: 50 μm.

flow, leading to the development of smaller seeds than WT. Although callose partially blocked nutrient flow, mutant seeds were still formed, most likely because of other redundantly functioning callose-degrading enzymes at the site. By contrast, in the *OEAtBG_ppap* seeds, callose was constitutively degraded, producing larger seeds because of the enhanced nutrient transport.

OEAtBGppap produces larger seeds even without fertilization

The *Arabidopsis* mutant *fertilization-independent seed 2* (*fis2*) produces an autonomous endosperm without fertilization.[44] However, it is unclear why autonomous endosperm mutants produce seeds as large as those produced by the WT. Therefore, the relationship between the autonomous endosperm and the PE was further investigated using aniline blue staining. Callose was degraded in the WT but was deposited in *gcs1* ovules (Figures 5I and 5J); however, callose in *fis2* was degraded even without fertilization (Figure 5K), indicating that autonomous endosperm formation was sufficient to remove callose and obtain nutrients via the phloem. This also suggests that the activation of the central cell for endosperm cell proliferation in *fis2* also opens the gate, explaining why autonomous endosperm mutants produce seeds as large as those produced by WT. To investigate whether *OEAtBG_ppap* (PE always open) plants can produce larger seeds, even without fertilization, the size of seeds from WT ovules crossed with *gcs1* pollen and *OEAtBG_ppap* ovules crossed with *gcs1* pollen were compared (Figure 5L). *OEAtBG_ppap* seeds without fertilization (POEM) were 7.2% (1 DAP), 30% (2 DAP), and 210% (3 DAP) larger than WT seeds without fertilization.

AtBG_ppap facilitates the flow of nutrients from PE to seed

Ultrastructural images from dissected ovules (Figures 6A–6I) with statistical comparisons (Figures 6J and 6K) showed that NPT ovules had small starch grains (Figures 6B and 6F), while

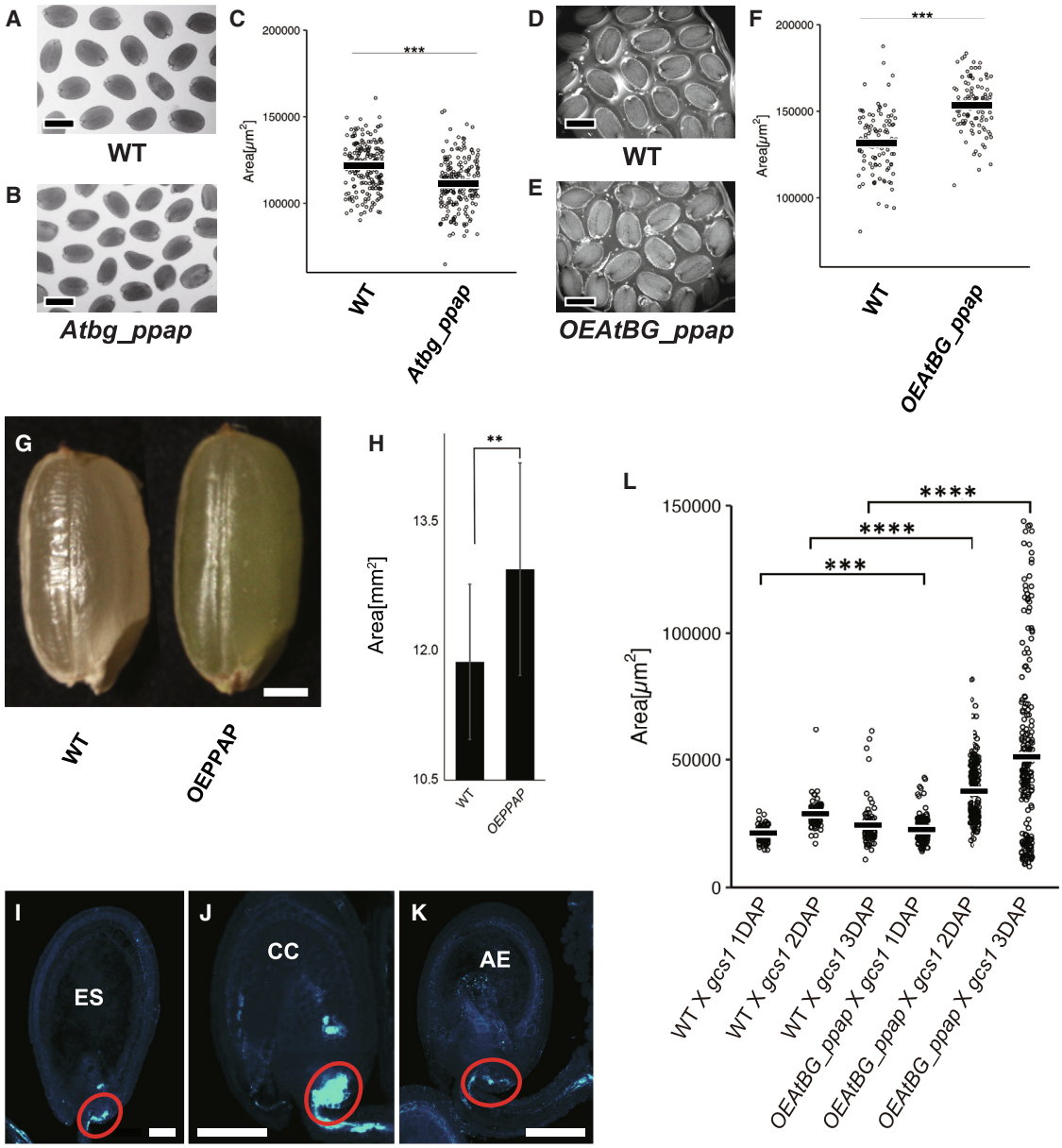

Figure 5. Seed size modification by the PE and PPAP in *Arabidopsis* and rice

(A and B) Actual seeds in the WT (A) and *Atbg_ppap* (B).

(C) WT seed size: $1.21 \times 10^5 \pm 0.13 \times 10^5$ μm^2 (mean ± SD; $n = 200$ seeds), *Atbg_ppap* seed size: $1.11 \times 10^5 \pm 1.45$ μm^2 ($n = 200$ seeds). *Atbg_ppap* seeds were 8.4% smaller than those of WT. Welch's two-sample t test was used to assess the significance of differences. ***$p < 0.001$.

(D and E) Actual seeds in WT (D) and *OEAtBG_ppap* (E).

(F) WT seed size: $1.32 \times 10^5 \pm 0.18 \times 10^5$ μm^2 ($n = 200$ seeds), *OEAtBG_ppap* seed size: $1.53 \times 10^5 \pm 0.15 \times 10^5$ μm^2 ($n = 200$ seeds). *OEAtBG_ppap* seeds were 16.5% larger than those of WT. Welch's two-sample t test was used to assess the significance of differences. ***$p < 0.001$.

(G) A mature Nipponbare rice seed (left) and a seed overexpressing a *PPAP* gene (*OEPPAP*) (right). (H) Nipponbare seed size: 11.86 ± 0.9 mm^2 ($n = 32$ seeds), *OEPPAP* seed size: 12.93 ± 1.23 mm^2 ($n = 32$ seeds). Welch's two-sample t test was used to assess the significance of differences. **$p < 0.01$.

(I–K) Results of aniline blue staining for WT (I), *gcs1* (J), and *fis2* (K) ovules. Weak callose deposition in the WT (I) but intensive deposition in *gcs1* (J). Weak callose deposition in *fis2* without fertilization (K).

(L) The mean size of WT × *gcs1* seeds was $2.11 \times 10^4 \pm 0.28 \times 10^4$ μm^2 ($n = 97$ seeds) at 1 DAP, $2.89 \times 10^4 \pm 0.46 \times 10^4$ μm^2 ($n = 109$ seeds) at 2 DAP, and $2.43 \times 10^4 \pm 0.84 \times 10^4$ μm^2 ($n = 82$ seeds) at 3 DAP. The size of *OEAtBG_ppap* × *gcs1* seeds was $2.26 \times 10^4 \pm 0.42 \times 10^4$ μm^2 ($n = 241$ seeds) at 1 DAP, $3.75 \times 10^4 \pm 1.14 \times 10^4$ μm^2 ($n = 249$ seeds) at 2 DAP, and $5.11 \times 10^4 \pm 3.41 \times 10^4$ μm^2 ($n = 220$ seeds) at 3 DAP. Welch's two-sample t test was used to assess the significance of differences. ***$p < 0.001$. ****$p < 0.0001$.

Scale bars: 500 μm (A, B, D, and E), 1 mm (G), and 50 μm (I–K).

ES, endosperm; CC, central cell; AE, autonomous endosperm.

See also Figures S2, S3, S7, and S8.

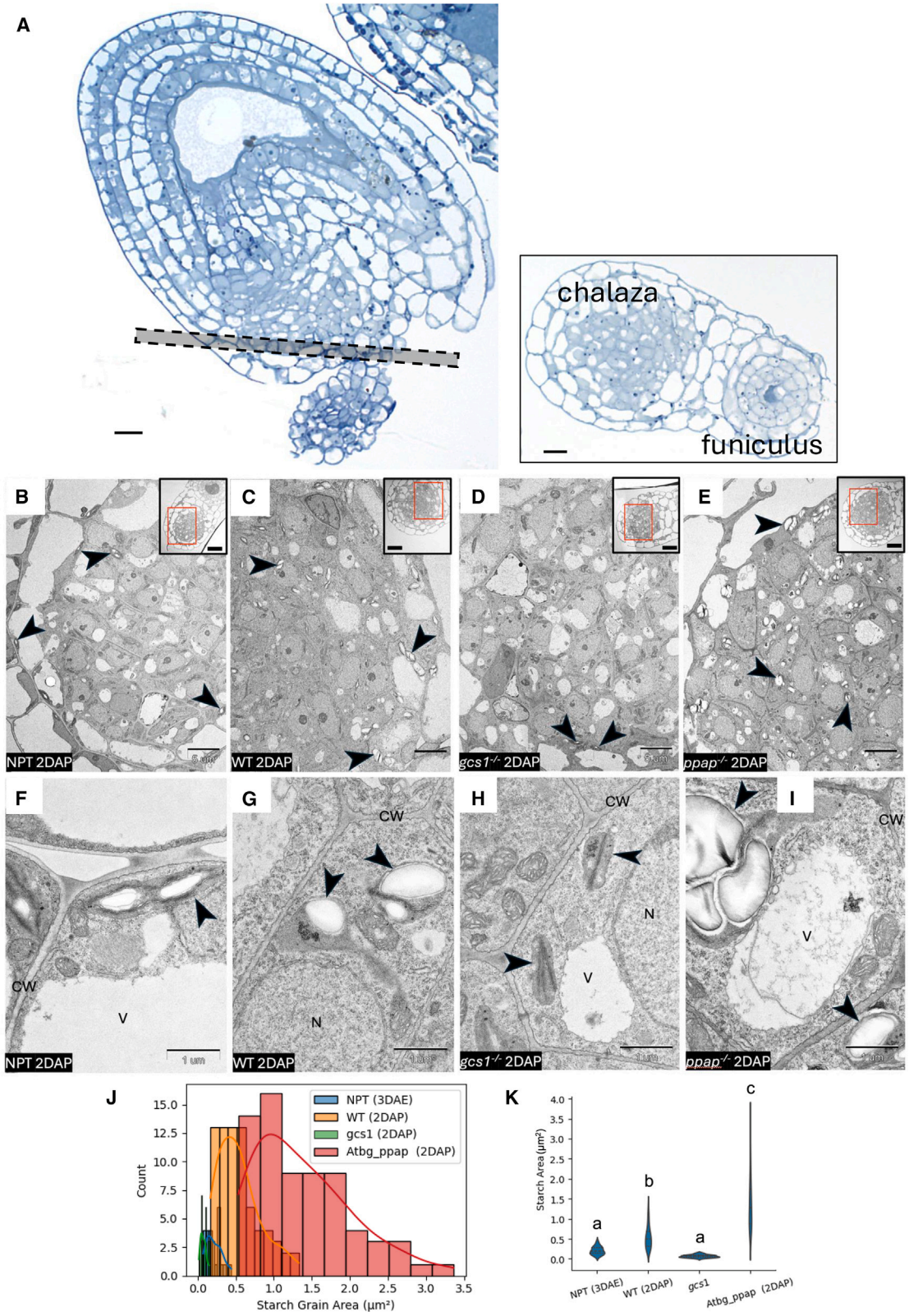

Figure 6. Ultrastructure analysis of the amyloplasts, nutrition flows for each ovule

The cells in the chalazal gate region exhibited discrepancies in their amyloplasts (arrowheads) depending on their fertilization state.

(A) A gray bar with dashed lines indicates where a section was made in an ovule through the chalazal end to the funiculus, as shown in the image at right.

(legend continued on next page)

fertilized ovules (or at least central cell fertilization) contained medium starch grains in their amyloplasts (Figures 6C and 6G), consistent with the surge in phloem unloading and inward photosynthate flow after fertilization (CF: Figure 3A; Video S6; esculin: Figure S6J). In the absence of fertilization, as observed in the *gcs1/gcs1* pollinated ovules (Figure 6D), the nutrient flow is not triggered but rather ceases (CF: Figure 3B; Video S7; esculin: Figure S6K), and the chalazal cell amyloplasts mostly appear to be devoid of starch grains (Figure 6H). By contrast, the fertilized *Atbg_ppap/Atbg_ppap* ovules (Figure 6E) had large starch grains in their amyloplasts (Figure 6I). These results strongly suggest that nutrient flow into the fertilized *Atbg_ppap/Atbg_ppap* ovules was triggered, but sugar efflux was blocked (Figure 3C; Video S8), leading to the accumulation of cellular starch in these cells. Unlike the *Atbg_ppap/Atbg_ppap* ovules, *gcs1/gcs1* ovules apparently have no phloem unloading at the chalazal end and therefore no starch in their amyloplasts. Consequently, we observed the abortion of the *gcs1/gcs1* ovules and a decrease in size of the *Atbg_ppap/Atbg_ppap* seeds. Our data also showed that plants sustain NPT ovules for least by 3 DAE.

Figure 7 presents a summary of this report for both *Arabidopsis* and rice seeds.

DISCUSSION

Nutrient flow to the developing seed is governed by the PE

Seed size is one of the most important traits in plant breeding, as it significantly influences crop yield. A key component and potential limiting factor of seed development is the supply of nutrients from the mother plant. These nutrients are delivered through the phloem, which ends in the maternal tissue where the funiculus joins the chalazal end of the ovule. As the phloem does not extend directly into the developing embryo or endosperm, all of the materials supplied by the phloem are first exported symplastically from the phloem into transfer cells and then into the apoplastic space separating the maternal and embryonic tissues before being taken up by transfer cells of the developing megagametophyte/endosperm.[45] Here, we demonstrated that the PE region in which this occurs is characterized by the presence of callose (Figure 1). At the time of fertilization, these cells contain moderate amounts of callose and form a circular structure associated with the PE. In addition, cells in the region opposite the PE where the endosperm will develop also exhibit higher callose content (Figure 1). Following fertilization, the callose content declines in both regions, but if fertilization does not occur, due to either absence of pollen (NPT) or to impaired pollen nuclei (*gcs1* pollen), callose content of both regions is maintained or increases, and further development of the ovule does not occur. The difference in the amount of callose deposition between NPT and *gcs1* ovules could be explained by the presence of pollen tube contents deposited in the ovules.[21] NPT ovules lack pollen tube content because of the absence of pollen tubes, indicating no sign of failed fertilization. Those ovules likely remain competent for fertilization, as other mechanisms allow only one pollen tube to enter the funiculus at a time.[46,47] However, in *gcs1* ovules in which the pollen tube enters into the synergid cell but the sperm nuclei are defective, we speculate that the ovules sense fertilization failure. The difference in the sensing mechanism between NPT and *gcs1* ovules likely accounts for the difference in callose deposition.

Identification of the new nutrition regulatory mechanism triggered by fertilization of the central cell

Previous studies have recognized the PE as a nutrient-unloading region.[6,14–17] However, the definitive structure of this region had been only partially identified. Our study demonstrated that callose deposition occurred in the PE, indicating that this region functions as a nutrient-unloading site. Reduction in the callose in this region was associated with successful fertilization of the central cell but not of the egg cell (Figure 4). While egg cell fertilization produces an embryo inheriting genetic information from both parents, it does not induce the opening of the PE gate. By contrast, central cell fertilization leading to endosperm cell proliferation does trigger gate opening, even without egg cell fertilization. As egg cell fertilization generally precedes central cell fertilization, this signaling from the central cell would tend to assure that both the egg and central cell had been fertilized. Following central cell fertilization, endosperm cells develop in proximity to the chalazal side of the ovule, across from the funiculus (Figure 7), and they also degrade callose in response to fertilization. An additional callose deposition site often observed at the base of the ovule's posterior end in the NPT and *gcs1* ovules is likely part of a regulatory system governing the uptake of nutrients unloaded at the PE and passed by the putative transfer cells bracketed by these two callose deposition sites (Figure 3G). By contrast, the embryo cells are located on the micropylar side of the ovule, away from the unloading region, perhaps explaining their lack of communication with the PE region. Moreover, as a nutrient reserve tissue that proliferates rapidly after fertilization, the endosperm generates a greater "energy sink," supporting the hypothesis that endosperm cells trigger gate opening. Polycomb group mutants, including *mea*,[48,49] *fis2*,[44] *fie*,[50] and *msi1*[51] mutants, produce autonomous endosperm development without fertilization and result in larger ovules than embryo-only ovules. In *fis2*, the autonomous endosperm exhibits less callose deposition at the chalazal end (Figure 5K), consistent with larger ovule formation. In addition, callose levels are similar in ovules with autonomous endosperm formation

(B) Unfertilized ovule (NPT) with few amyloplasts containing small starch grains at 2 DAP.
(C) Normally fertilized WT ovule with amyloplasts harboring relatively larger starch grains at 2 DAP.
(D) *gcs1*$^{-/-}$ pollinated ovule amyloplasts harbored almost no starch grains.
(E) *Atbg_ppap/−* ovule with amyloplasts containing much larger starch grains at 2 DAP.
(F–I) Magnified image of (B)–(E), respectively.
(J) Histogram of total starch grain counts and areas among samples from equal tissue area.
(K) Violin plot of the starch grain area in each sample. The different alphabets on the top indicate statistical significance ($p \leq 0.005$; n = 26–73; Tukey test).
Scale bars, (A) 10 μm; insets of (B)–(E), 20 μm; main images of (B)–(E), 5 μm; (F–I) 1 μm.
CW, cell wall; V, vacuole; N, nucleus. See also Figures S2 and S3.

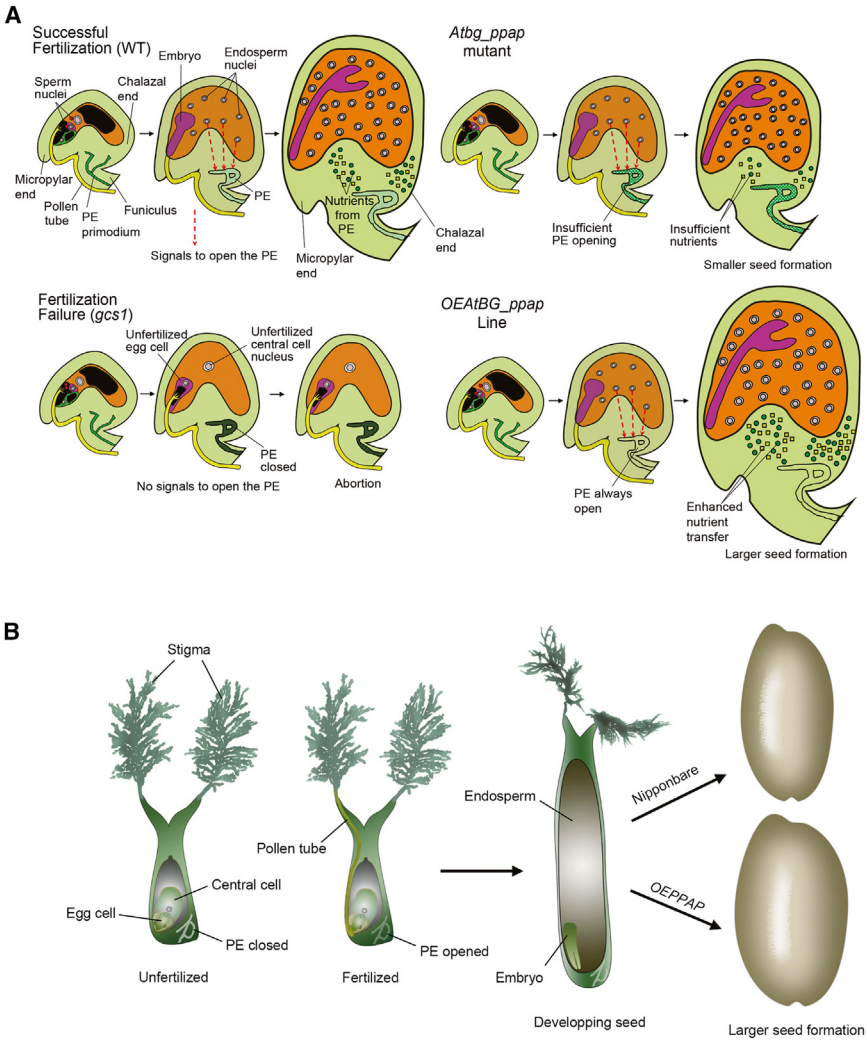

Figure 7. Seed size control via the PE

(A) *Arabidopsis*: at 1 DAP, all ovule types (WT, *gcs1*, *Atbg_ppap*, and *OEAtBG_ppap*) contain a PE primordium with branched phloem tubes; however, mature PE is formed at approximately 2 DAP. After fertilizing the central cell in WT, the cells (early endosperm) send fertilization completion signals to the PE. Subsequently, enzymes for callose degradation, including AtBG_ppap, degrade the callose in the PE, thus allowing the transport of nutrients to the fertilized ovule. In *gcs1*, as the fertilization of the central cell fails, the unfertilized cell does not send fertilization completion signals to the PE, and the callose degradation enzymes are not synthesized; thus, the PE continues to deposit callose without transporting nutrients, which results in the abortion of the ovule. In *Atbg_ppap*, the central cell is fertilized, and the early endosperm sends fertilization completion signals to the PE. However, as the AtBG_ppap protein is not functional, callose degradation remains incomplete. The partial callose deposition interferes with the PE nutrient transport system, resulting in the formation of smaller seeds. By contrast, the *OEAtBG_ppap* line constitutively expresses the AtBG_ppap enzyme, which degrades callose in the PE and facilitates nutrient flow from the funiculus to the ovule, producing larger seeds than those produced by WT. (B) *Oryza sativa*: the PE at the bottom of the pistil in rice has a similar structure to the PE in *Arabidopsis*. Callose deposition in an unfertilized pistil was greater than in a fertilized one. After fertilization, seeds overexpressing a gene encoding a *PPAP* (*OEPPAP*) grew to larger size than Nipponbare ones.

without fertilization and in ovules with central cell-only fertilization (Figure 4B), reinforcing the link between callose degradation and central cell fertilization.

Identification of the "key" enzyme, AtBG_ppap, to open the PE gate

As loss of callose was associated with successful seed development following fertilization, we identified genes encoding β-1,3-glucanase (a callose-degrading enzyme) through a homology search based on aa sequences. By comparing the expression profiles of all genes, we identified the *AtBG_ppap* gene, which was upregulated after fertilization in the WT but not in the unfertilized *gcs1* ovules. *AtBG_ppap* encodes a membrane-bound protein known to be involved in plasmodesmata gating via callose degradation.[28] We conducted a detailed investigation of nutrient flow using live-cell imaging of the CF dye tracer marker (Figure 3). In unfertilized *gcs1* ovules, no signal was detected in the main body of the ovule, whereas *Atbg_ppap* ovules showed a faint signal in the main body. These results suggest that in *gcs1* ovules, nutrient flow is completely blocked by accumulated callose, resulting in seed abortion. However, in the *Atbg_ppap* ovules, nutrition is only partially impeded by callose deposition, producing smaller seeds but with germination potential (Figure 5B). We propose that *gcs1* ovules exhibit a complete shutdown of nutrient flow because the callose degradation enzyme was not upregulated in the absence of fertilization. By contrast, judging from the difference in callose deposition amount between *Atbg_ppap* and *gcs1* ovules, *Atbg_ppap* can still produce smaller but viable seeds, possibly due to the more limited action of additional BGs. We also observed that *OEAtBG_ppap* ovules can enlarge without fertilization using *gcs1* pollen. Similar to *fis2*, *OEAtBG_ppap* ovules can degrade callose without fertilization and obtain nutrients via the gate, enlarging ovule size.

Visualization of the CFDA and esculin flow at the PE gate

Since AtBG_ppap is known to be a membrane-bound protein involved in callose degradation in the plasmodesmata,[28] it is reasonable to assume that its defective mutants compromise the symplastic system. This is consistent with our observation of symplastic tracer CFDA flow across the phloem unloading site in fertilized and unfertilized ovules. Furthermore, a similar observation was made with esculin, a tracer for sugar transport, indicating that the initial nutrient (or at least sugar) flow to the ovule occurs mainly through the symplastic pathway. However, both symplastic and apoplasmic flows of nutrients have been proposed during fruit and seed development, with the latter

initiating relatively later during the process.[52,53] This could be why the *Atbg_ppap* still produced seeds, albeit with reduced size. Alternatively, unidentified redundant AtBG_ppap-like proteins might play a role in this process. The differences between ovule/seed development in the NPT/*gcs1* and *Atbg_ppap* lines also suggest that initial symplastic flow is crucial for signal exchange between the reproductive and non-reproductive tissues, which could be linked to the initiation of symplastic nutrient flow afterward. Alternatively, the nutrient flow to the ovule could be regulated by the combination of both symplastic and apoplastic pathways. A review in 1994 postulated the presence of a "modified cell wall acting as the semipermeable apoplastic membranes at the phloem unloading region to allow the passage of solutes toward the developing seeds selectively."[54] It is possible that the callose deposited at the posterior end of the ovule acts to contain nutrients released into the apoplast as they pass from the maternal tissue to the embryonic transfer cells and to further symplastic flow within the developing seeds. The ability of callose to confer semi-permeability to cell walls (i.e., permeable to water but not to solutes) was demonstrated for the perisperm envelope of the muskmelon (*Cucumis melo*) seed, which contains callose in its cell walls that determine the semi-permeability of the envelope.[55] However, whether callose-deposited cell walls function as such permeable apoplastic membranes at the PE remains unknown. Further research is required to confirm whether this is the case and shed more light on the entire mechanism of nutrient flow during seed formation.

Seed size modification by AtBG_ppap in *Arabidopsis* and rice

Unlike other seed size-modulating genes, including plant hormone-related and cell metabolism-related proteins,[1,2] the molecular mechanism of action of most of the products of these genes is yet to be understood. By contrast, seed size modification by AtBG_ppap is well explained by the nutrient flows governed by the callose-blocking system. If a single aa transporter, UmamiT, is missing, 12% smaller seeds were observed.[6] This observation is reasonable because these seeds lack sufficient amounts of aa. However, UmamiT overexpression cannot be applied to enlarge seeds because seeds require multiple nutrients, and increased amounts of a single aa cannot compensate for all nutrients. By contrast, overexpression of AtBG_ppap can be used to enlarge the seed because the protein physically removes callose deposits, which apparently allows transportation of all nutrients from the PE into the seeds. We additionally assessed the presence of callose deposition in differentially fertilized rice ovules (Figure 2). Interestingly, a very similar structure to that in the *Arabidopsis* ovules was observed in rice ovules, suggesting potential conservation of the structure-dependent mechanism of nutrient flow at least in the angiosperms. Exploitation of this structure for more efficient nutrient flow toward the developing seeds/ovules holds promise for increasing yields in the seed crops (Figure 5). So far, AtBG_ppap is one of the strong candidates for modifying seed size by controlling callose deposition/degradation in *Arabidopsis* (dicots) and *Oryza sativa* (monocots), covering angiosperms widely. From a commercial viewpoint, only one gene modification could be sufficient to increase or reduce the seed size in seed and fruit crops.

Identification of the wise plant strategy: The callose-blocking system

In our previous work, we unveiled a fertilization recovery system wherein a second pollen tube can compensate for the failure of the first pollen tube in fertilization.[56–58] This system reflects a strategic approach by plants to maximize seed yield, enabling ovules to be fertilized via a second pollen tube in cases of initial failure. Building on this concept, this study reveals another plant strategy involving the callose-blocking system. Supplying nutrients to unfertilized ovules in plants would be energetically wasteful, given their inability to develop into a viable seed. Thus, prioritizing nutrient supply to fertilized ovules is essential for the most efficient use of plant resources. To prevent nutrient wastage, plants have evolved a mechanism that blocks nutrient flow until the ovule detects completed fertilization. Ultrastructural analysis showed that successful fertilization triggers the phloem unloading and inward flow of nutrients. In the absence of fertilization, the nutrient flow was not triggered. The defect in AtBG_ppap did not prevent all nutrient entry but blocked sugar efflux, resulting in smaller seed size. We confirmed that *AtBG_ppap* is one of the key genes playing a role in regulating the nutrient flow efficiency from the mother plant into the developing ovule. Our study emphasizes the critical role of the initial symplastic and/or apoplastic passage from the phloem in this process. Further research is needed to fully understand this mechanism and explore how plants finely regulate nutrient allocation to optimize seed production while conserving resources. Future studies should determine the molecular mechanisms underlying the recognition of central cell fertilization and the signaling that controls callose deposition as well as identify the cellular localization of AtBG_ppap and its relationship to fertilization and ovule callose content and assess whether additional BGs may be involved.

RESOURCE AVAILABILITY

Lead contact

Requests for further information and resources should be directed to and will be fulfilled by the lead contact, Ryushiro D. Kasahara (kasahara.ryushiro.s2@f.mail.nagoya-u.ac.jp).

Materials availability

This study did not generate new, unique reagents.

Data and code availability

- All data reported in this paper will be shared by the lead contact upon request.
- This paper does not report original code.
- Any additional information required to reanalyze the data reported in this paper is available from the lead contact upon request.

ACKNOWLEDGMENTS

We thank Maki Hattori, Aidi Xu, and Wei Xia for technical assistance. This work was supported by Japan Society for the Promotion of Science Grants-in-Aid for Scientific Research (grant no. 22K21366 to R.D.K.); start-up funds from the School of Life Sciences, Fujian Agriculture and Forestry University (grant no. 114-712018008 to R.D.K.); and the FAFU-UCR Joint Center, Haixia Institute of Science and Technology, Fujian Agriculture and Forestry University (grant no. 102-118990010 to R.D.K.). This work was also supported by the Chinese NSFC fund (grant #: 31970809 to R.D.K.). This work was also supported by the Precursory Research for Embryonic Science and Technology (grant no.

13416724 to R.D.K.; Kasahara Sakigake Project, Japan Science and Technology Agency to R.D.K.). This work was partially supported by the Carbon Recycle Foundation (grant no. 5-01-2024 to R.D.K.). This work was partially supported by the Japan Society for the Promotion of Science Grants-in-Aid for Scientific Research (grant nos. 19H05361, 20H03273, 21H00368, 23H04196, and 24K02043 to M. Notaguchi and 16H06464 and 16K21727 to T.H.).

AUTHOR CONTRIBUTIONS

M. Notaguchi and R.D.K. conceptualized the study. X.L. and R.D.K. discovered the seed nutrition regulatory system. K.P.N. conducted all the live-cell imaging experiments. X.L., P.B.A., M. Notaguchi, and R.D.K. designed the experiments. P.B.A., T.K., K.Y., and Y.K. conducted all the phenotypic observations in rice. X.W., S.Z., and P.B.A. created *OEAtBG_ppap* and complementation lines. T.I. created the *Atbg_ppap* mutant by CRISPR. X.L., K.P.N., X.W., S.Z., P.B.A., L.X., C.H., J.H., and R.D.K. performed the phenotypic analysis of *Atbg_ppap* mutant and *OEAtBG_ppap* lines. K.O. and R.D.K. performed the expression analysis for these lines. M. Nakamura created the SWEET10 promoter-driven GFP line. K.-i.K. and M. Notaguchi conducted the SWEET protein analysis. P.B.A. conducted the PE ultrastructure analysis. X.L., Y.S., and R.D.K. performed detailed phenotypic analysis for the PE callose deposition. X.L. and P.B.A. performed phenotypic analysis of esculin flow experiments. S.S., T.H., K.J.B., M. Notaguchi, and R.D.K. wrote the paper from the input of all authors' experimental results.

DECLARATION OF INTERESTS

Nagoya University has filed for a patent regarding the following topic: "modified plant formation." R.D.K., K.-i.K., and M. Notaguchi are inventors related to patent application no. JP2023-115896.

STAR★METHODS

Detailed methods are provided in the online version of this paper and include the following:

- KEY RESOURCES TABLE
- EXPERIMENTAL MODEL AND STUDY PARTICIPANT DETAILS
  - Plant materials and growth conditions
- METHOD DETAILS
  - Construction of *Atbg_ppap* mutant and *OEAtBG_ppap* lines
  - Construction of AtSWEET10-GFP line
  - The phloem end phenotypic analyses
  - CFDA and esculin
  - Vector preparation for rice
  - Rice transformation and regeneration
  - Observation of rice pistils
- QUANTIFICATION AND STATISTICAL ANALYSIS
  - Quantification
  - Statistical analysis

SUPPLEMENTAL INFORMATION

Supplemental information can be found online at https://doi.org/10.1016/j.cub.2025.03.033.

Received: August 17, 2024
Revised: January 9, 2025
Accepted: March 17, 2025
Published: April 7, 2025

REFERENCES

1. Orozco-Arroyo, G., Paolo, D., Ezquer, I., and Colombo, L. (2015). Networks controlling seed size in Arabidopsis. Plant Reprod. *28*, 17–32. https://doi.org/10.1007/s00497-015-0255-5.
2. Li, N., Xu, R., and Li, Y. (2019). Molecular networks of seed size control in plants. Annu. Rev. Plant Biol. *70*, 435–463. https://doi.org/10.1146/annurev-arplant-050718-095851.
3. Di Marzo, M., Babolin, N., Viana, V.E., de Oliveira, A.C., Gugi, B., Caporali, E., Herrera-Ubaldo, H., Martínez-Estrada, E., Driouich, A., de Folter, S., et al. (2022). The Genetic control of SEEDSTICK and LEUNIG-HOMOLOG in seed and fruit development: New insights into cell wall control. Plants (Basel) *11*, 3146. https://doi.org/10.3390/plants11223146.
4. Gomez, M.D., Cored, I., Barro-Trastoy, D., Sanchez-Matilla, J., Tornero, P., and Perez-Amador, M.A. (2023). DELLA proteins positively regulate seed size in Arabidopsis. Development *150*, dev201853. https://doi.org/10.1242/dev.201853.
5. Bai, C., Wang, G.J., Feng, X.H., Gao, Q., Wang, W.Q., Xu, R., Guo, S.J., Shen, S.Y., Ma, M., Lin, W.H., et al. (2024). OsMAPK6 phosphorylation and CLG ubiquitylation of GW6a non-additively enhance rice grain size through stabilization of the substrate. Nat. Commun. *15*, 4300. https://doi.org/10.1038/s41467-024-48786-0.
6. Müller, B., Fastner, A., Karmann, J., Mansch, V., Hoffmann, T., Schwab, W., Suter-Grotemeyer, M., Rentsch, D., Truernit, E., Ladwig, F., et al. (2015). Amino acid export in developing Arabidopsis seeds depends on UmamiT facilitators. Curr. Biol. *25*, 3126–3131. https://doi.org/10.1016/j.cub.2015.10.038.
7. Dumas, C., and Rogowsky, P. (2008). Fertilization and early seed formation. C. R. Biol. *331*, 715–725. https://doi.org/10.1016/j.crvi.2008.07.013.
8. Hands, P., Rabiger, D.S., and Koltunow, A.M. (2016). Mechanisms of endosperm initiation. Plant Reprod. *29*, 215–225. https://doi.org/10.1007/s00497-016-0290-x.
9. Dresselhaus, T., Sprunck, S., and Wessel, G.M. (2016). Fertilization mechanisms in flowering plants. Curr. Biol. *26*, R125–R139. https://doi.org/10.1016/j.cub.2015.12.032.
10. Adhikari, P.B., Liu, X., Wu, X., Zhu, S., and Kasahara, R.D. (2020). Fertilization in flowering plants: an odyssey of sperm cell delivery. Plant Mol. Biol. *103*, 9–32. https://doi.org/10.1007/s11103-020-00987-z.
11. Koltunow, A.M., and Grossniklaus, U. (2003). APOMIXIS: A developmental perspective. Annu. Rev. Plant Biol. *54*, 547–574. https://doi.org/10.1146/annurev.arplant.54.110901.160842.
12. Underwood, C.J., and Mercier, R. (2022). Engineering apomixis: clonal seeds approaching the fields. Annu. Rev. Plant Biol. *73*, 201–225. https://doi.org/10.1146/annurev-arplant-102720-013958.
13. Khanday, I., Santos-Medellín, C., and Sundaresan, V. (2023). Somatic embryo initiation by rice BABY BOOM1 involves activation of zygote-expressed auxin biosynthesis genes. New Phytol. *238*, 673–687. https://doi.org/10.1111/nph.18774.
14. Stadler, R., Lauterbach, C., and Sauer, N. (2005). Cell-to-cell movement of green fluorescent protein reveals post-phloem transport in the outer integument and identifies symplastic domains in Arabidopsis seeds and embryos. Plant Physiol. *139*, 701–712. https://doi.org/10.1104/pp.105.065607.
15. Werner, D., Gerlitz, N., and Stadler, R. (2011). A dual switch in phloem unloading during ovule development in Arabidopsis. Protoplasma *248*, 225–235. https://doi.org/10.1007/s00709-010-0223-8.
16. Vogiatzaki, E., Baroux, C., Jung, J.Y., and Poirier, Y. (2017). PHO1 exports phosphate from the chalazal seed coat to the embryo in developing Arabidopsis seeds. Curr. Biol. *27*, 2893–2900.e3. https://doi.org/10.1016/j.cub.2017.08.026.
17. Karmann, J., Müller, B., and Hammes, U.Z. (2018). The long and winding road: transport pathways for amino acids in Arabidopsis seeds. Plant Reprod. *31*, 253–261. https://doi.org/10.1007/s00497-018-0334-5.
18. Mori, T., Kuroiwa, H., Higashiyama, T., and Kuroiwa, T. (2006). GENERATIVE CELL SPECIFIC 1 is essential for angiosperm fertilization. Nat. Cell Biol. *8*, 64–71. https://doi.org/10.1038/ncb1345.
19. von Besser, K., Frank, A.C., Johnson, M.A., and Preuss, D. (2006). Arabidopsis *HAP2* (*GCS1*) is a sperm-specific gene required for pollen

tube guidance and fertilization. Development *133*, 4761–4769. https://doi.org/10.1242/dev.02683.

20. Nagahara, S., Takeuchi, H., and Higashiyama, T. (2015). Generation of a homozygous fertilization-defective *gcs1* mutant by heat-inducible removal of a rescue gene. Plant Reprod. *28*, 33–46. https://doi.org/10.1007/s00497-015-0256-4.
21. Kasahara, R.D., Notaguchi, M., Nagahara, S., Suzuki, T., Susaki, D., Honma, Y., Maruyama, D., and Higashiyama, T. (2016). Pollen tube contents initiate ovule enlargement and enhance seed coat development without fertilization. Sci. Adv. *2*, e1600554. https://doi.org/10.1126/sciadv.1600554.
22. Kasahara, R.D., Notaguchi, M., and Honma, Y. (2017). Discovery of pollen tube-dependent ovule enlargement morphology phenomenon, a new step in plant reproduction. Commun. Integr. Biol. *10*, 4. https://doi.org/10.1080/19420889.2017.1338989.
23. Zhong, S., Zhang, J., and Qu, L.-J. (2017). The signals to trigger the initiation of ovule enlargement are from the pollen tubes: The direct evidence. J. Integr. Plant Biol. *59*, 600–603. https://doi.org/10.1111/jipb.12577.
24. Liu, X., and Kasahara, D.R.D. (2023). Reproductive Strategies of the Female Gametophyte (IntechOpen), p. 109805. https://doi.org/10.5772/intechopen.109805.
25. Liu, X., Adhikari, P.B., and Kasahara, R.D. (2023). Pollen Tube Content Facilitates and Increases the Potential of Endosperm Proliferation Irrespective of Fertilization in *Arabidopsis thaliana*. Cytologia *88*, 35–39. https://doi.org/10.1508/cytologia.88.35.
26. Thorne, J.H. (1981). Morphology and ultrastructure of maternal seed tissues of soybean in relation to the import of photosynthate. Plant Physiol. *67*, 1016–1025. https://doi.org/10.1104/pp.67.5.1016.
27. Patrick, J.W., and Offler, C.E. (2001). Compartmentation of transport and transfer events in developing seeds. J. Exp. Bot. *52*, 551–564. https://doi.org/10.1093/jexbot/52.356.551.
28. Levy, A., Erlanger, M., Rosenthal, M., and Epel, B.L. (2007). A plasmodesmata-associated β-1,3-glucanase in Arabidopsis. Plant J. *49*, 669–682. https://doi.org/10.1111/j.1365-313X.2006.02986.x.
29. Paterlini, A., Dorussen, D., Fichtner, F., van Rongen, M., Delacruz, R., Vojnović, A., Helariutta, Y., and Leyser, O. (2021). Callose accumulation in specific phloem cell types reduces axillary bud growth in *Arabidopsis thaliana*. New Phytol. *231*, 516–523. https://doi.org/10.1111/nph.17398.
30. Hough, T., Bernhardt, P., Knox, R.B., and Williams, E.G. (1985). Applications of fluorochromes to pollen biology. II. The DNA probes ethidium bromide and Hoechst 33258 in conjunction with the callose specific aniline blue fluorochrome. Stain Technol. *60*, 155–162. https://doi.org/10.3109/10520298509113906.
31. Mizuta, Y., Kurihara, D., and Higashiyama, T. (2015). Two-photon imaging with longer wavelength excitation in intact Arabidopsis tissues. Protoplasma *252*, 1231–1240. https://doi.org/10.1007/s00709-014-0754-5.
32. Noll, G.A., Rüping, B., Ernst, A.M., Bucsenez, M., Twyman, R.M., Fischer, R., and Prüfer, D. (2009). The promoters of forisome genes *MtSEO2* and *MtSEO3* direct gene expression to immature sieve elements in *Medicago truncatula* and *Nicotiana tabacum*. Plant Mol. Biol. Rep. *27*, 526–533. https://doi.org/10.1007/s11105-009-0120-5.
33. Froelich, D.R., Mullendore, D.L., Jensen, K.H., Ross-Elliott, T.J., Anstead, J.A., Thompson, G.A., Pélissier, H.C., and Knoblauch, M. (2011). Phloem ultrastructure and pressure flow: Sieve-element-occlusion-related agglomerations do not affect translocation. Plant Cell *23*, 4428–4445. https://doi.org/10.1105/tpc.111.093179.
34. Honma, Y., Adhikari, P.B., Kuwata, K., Kagenishi, T., Yokawa, K., Notaguchi, M., Kurotani, K., Toda, E., Bessho-Uehara, K., Liu, X., et al. (2020). High-quality sugar production by osgcs1 rice. Commun. Biol. *3*, 617. https://doi.org/10.1038/s42003-020-01329-x.
35. Andrés, F., Kinoshita, A., Kalluri, N., Fernández, V., Falavigna, V.S., Cruz, T.M.D., Jang, S., Chiba, Y., Seo, M., Mettler-Altmann, T., et al. (2020). The sugar transporter SWEET10 acts downstream of FLOWERING LOCUS T during floral transition of *Arabidopsis thaliana*. BMC Plant Biol. *20*, 53. https://doi.org/10.1186/s12870-020-2266-0.
36. Chen, L., Ganguly, D.R., Shafik, S.H., Danila, F., Grof, C.P.L., Sharwood, R.E., and Furbank, R.T. (2023). The role of SWEET4 proteins in the post-phloem sugar transport pathway of *Setaria viridis* sink tissues. J. Exp. Bot. *74*, 2968–2986. https://doi.org/10.1093/jxb/erad076.
37. Oparka, K.J., Duckett, C.M., Prior, D.A.M., and Fisher, D.B. (1994). Real-time imaging of phloem unloading in the root tip of Arabidopsis. Plant J. *6*, 759–766. https://doi.org/10.1046/j.1365-313X.1994.6050759.x.
38. Roberts, A.G., Cruz, S.S., Roberts, I.M., Prior, D.A.M., Turgeon, R., and Oparka, K.J. (1997). Phloem unloading in sink leaves of *Nicotiana benthamiana*: Comparison of a fluorescent solute with a fluorescent virus. Plant Cell *9*, 1381–1396. https://doi.org/10.1105/tpc.9.8.1381.
39. Ron, M., Alandete Saez, M., Eshed Williams, L., Fletcher, J.C., and McCormick, S. (2010). Proper regulation of a sperm-specific cis-nat-siRNA is essential for double fertilization in Arabidopsis. Genes Dev. *24*, 1010–1021. https://doi.org/10.1101/gad.1882810.
40. Gooh, K., Ueda, M., Aruga, K., Park, J., Arata, H., Higashiyama, T., and Kurihara, D. (2015). Live-cell imaging and optical manipulation of Arabidopsis early embryogenesis. Dev. Cell *34*, 242–251. https://doi.org/10.1016/j.devcel.2015.06.008.
41. Kang, I.H., Steffen, J.G., Portereiko, M.F., Lloyd, A., and Drews, G.N. (2008). The AGL62 MADS domain protein regulates cellularization during endosperm development in Arabidopsis. Plant Cell *20*, 635–647. https://doi.org/10.1105/tpc.107.055137.
42. Knox, K., Paterlini, A., Thomson, S., and Oparka, K. (2018). The coumarin glucoside, esculin, reveals rapid changes in phloem-transport velocity in response to environmental cues. Plant Physiol. *178*, 795–807. https://doi.org/10.1104/pp.18.00574.
43. Rottmann, T.M., Fritz, C., Lauter, A., Schneider, S., Fischer, C., Danzberger, N., Dietrich, P., Sauer, N., and Stadler, R. (2018). Protoplast-esculin assay as a new method to assay plant sucrose transporters: characterization of AtSUC6 and AtSUC7 sucrose uptake activity in Arabidopsis Col-0 ecotype. Front. Plant Sci. *9*, 430. https://doi.org/10.3389/fpls.2018.00430.
44. Luo, M., Bilodeau, P., Koltunow, A., Dennis, E.S., Peacock, W.J., and Chaudhury, A.M. (1999). Genes controlling fertilization-independent seed development in *Arabidopsis thaliana*. Proc. Natl. Acad. Sci. USA *96*, 296–301. https://doi.org/10.1073/pnas.96.1.296.
45. Offler, C.E., and Patrick, J.W. (1993). Pathway of photosynthate transfer in the developing seed of *Vicia faba* L.: A structural assessment of the role of transfer cells in unloading from the seed coat. J. Exp. Bot. *44*, 711–724. https://doi.org/10.1093/jxb/44.4.711.
46. Higashiyama, T., and Yang, W.C. (2017). Gametophytic pollen tube guidance: Attractant peptides, gametic controls, and receptors. Plant Physiol. *173*, 112–121. https://doi.org/10.1104/pp.16.01571.
47. Mizuta, Y., and Higashiyama, T. (2018). Chemical signaling for pollen tube guidance at a glance. J. Cell Sci. *131*, jcs208447. https://doi.org/10.1242/jcs.208447.
48. Chaudhury, A.M., Ming, L., Miller, C., Craig, S., Dennis, E.S., and Peacock, W.J. (1997). Fertilization-independent seed development in *Arabidopsis thaliana*. Proc. Natl. Acad. Sci. USA *94*, 4223–4228. https://doi.org/10.1073/pnas.94.8.4223.
49. Grossniklaus, U., Vielle-Calzada, J.P., Hoeppner, M.A., and Gagliano, W.B. (1998). Maternal control of embryogenesis by *MEDEA*, a polycomb group gene in Arabidopsis. Science *280*, 446–450. https://doi.org/10.1126/science.280.5362.446.
50. Ohad, N., Yadegari, R., Margossian, L., Hannon, M., Michaeli, D., Harada, J.J., Goldberg, R.B., and Fischer, R.L. (1999). Mutations in *FIE*, a WD polycomb group gene, allow endosperm development without fertilization. Plant Cell *11*, 407–416. https://doi.org/10.1105/tpc.11.3.407.
51. Guitton, A.E., and Berger, F. (2005). Loss of function of MULTICOPY SUPPRESSOR OF IRA 1 produces nonviable parthenogenetic embryos in Arabidopsis. Curr. Biol. *15*, 750–754. https://doi.org/10.1016/j.cub.2005.02.066.

52. Lafon-Placette, C., and Köhler, C. (2014). Embryo and endosperm, partners in seed development. Curr. Opin. Plant Biol. *17*, 64–69. https://doi.org/10.1016/j.pbi.2013.11.008.

53. Ma, S., Li, Y., Li, X., Sui, X., and Zhang, Z. (2019). Phloem unloading strategies and mechanisms in crop fruits. J. Plant Growth Regul. *38*, 494–500. https://doi.org/10.1007/s00344-018-9864-1.

54. Bradford, K.J. (1994). Water stress and the water relations of seed development – a critical-review. Crop Sci. *34*, 1–11. https://doi.org/10.2135/cropsci1994.0011183X003400010001x.

55. Yim, K.O., and Bradford, K.J. (1998). Callose deposition is responsible for apoplastic semipermeability of the endosperm envelope of muskmelon seeds. Plant Physiol. *118*, 83–90. https://doi.org/10.1104/pp.118.1.83.

56. Kasahara, R.D., Maruyama, D., Hamamura, Y., Sakakibara, T., Twell, D., and Higashiyama, T. (2012). Fertilization recovery after defective sperm cell release in Arabidopsis. Curr. Biol. *22*, 1084–1089. https://doi.org/10.1016/j.cub.2012.03.069.

57. Beale, K.M., Leydon, A.R., and Johnson, M.A. (2012). Gamete fusion is required to block multiple pollen tubes from entering an Arabidopsis ovule. Curr. Biol. *22*, 1090–1094. https://doi.org/10.1016/j.cub.2012.04.041.

58. Kasahara, R.D., Maruyama, D., and Higashiyama, T. (2013). Fertilization recovery system is dependent on the number of pollen grains for efficient reproduction in plants. Plant Signal. Behav. *8*, e23690. https://doi.org/10.4161/psb.23690.

59. Miyashima, S., Koi, S., Hashimoto, T., and Nakajima, K. (2011). Non-cell-autonomous microRNA165 acts in a dose-dependent manner to regulate multiple differentiation status in the Arabidopsis root. Development *138*, 2303–2313. https://doi.org/10.1242/dev.060491.

60. Fauser, F., Schiml, S., and Puchta, H. (2014). Both CRISPR/Cas-based nucleases and nickases can be used efficiently for genome engineering in *Arabidopsis thaliana*. Plant J. *79*, 348–359. https://doi.org/10.1111/tpj.12554.

61. Yamaguchi, Y.L., Ishida, T., Yoshimura, M., Imamura, Y., Shimaoka, C., and Sawa, S. (2017). A collection of mutants for CLE-peptide-encoding genes in Arabidopsis generated by CRISPR/Cas9-mediated gene targeting. Plant Cell Physiol. *58*, 1848–1856. https://doi.org/10.1093/pcp/pcx139.

62. Shimozono, S., and Miyawaki, A. (2008). Engineering FRET constructs using CFP and YFP. Methods Cell Biol. *85*, 381–393. https://doi.org/10.1016/S0091-679X(08)85016-9.

63. Clough, S.J., and Bent, A.F. (1998). Floral dip: a simplified method for Agrobacterium-mediated transformation of *Arabidopsis thaliana*. Plant J. *16*, 735–743. https://doi.org/10.1046/j.1365-313x.1998.00343.x.

64. Christensen, C.A., King, E.J., Jordan, J.R., and Drews, G.N. (1997). Megagametogenesis in Arabidopsis wild type and the Gf mutant. Sex. Plant Reprod. *10*, 49–64. https://doi.org/10.1007/s004970050067.

STAR★METHODS

KEY RESOURCES TABLE

REAGENT or RESOURCE	SOURCE	IDENTIFIER
Biological samples		
gcs1/gcs1 homozygous	Nagahara et al.[20]	https://link.springer.com/article/; https://doi.org/10.1007/s00497-015-0256-4
RPS5Apro::tdTomato-LTI6b	Mizuta et al.[31]	https://link.springer.com/article/; https://doi.org/10.1007/s00709-014-0754-5
kpl/kpl homozygous	Ron et al.[39]	https://genesdev.cshlp.org/content/24/10/1010.long
WOX2p::H2B-GFP + WOX2p::LTI-tdTomato double marker	Gooh et al.[40]	https://www.sciencedirect.com/science/article/pii/S1534580715003974
AGL62::GFP	Kang et al.[41]	https://pmc.ncbi.nlm.nih.gov/articles/PMC2329934/
Chemicals, peptides, and recombinant proteins		
5(6)-carboxyfluorescein diacetate (CFDA)	Sigma	C8166
Esculin	Sigma	66778-17-4
Aniline Blue	Fujifilm Wako	015-18045
Oligonucleotides		
Primers	Listed in Table S1	N/A
Recombinant DNA		
pCAMBIA-1380 vector	Abcam	ab275769
pBIN40 vector	Miyashima et al.[59]	https://journals.biologists.com/dev/article/138/11/2303/44396/Non-cell-autonomous-microRNA165-acts-in-a-dose
Software and algorithms		
ImageJ (Fiji)	National Institute of Health	http://fiji.sc/

EXPERIMENTAL MODEL AND STUDY PARTICIPANT DETAILS

Plant materials and growth conditions

Arabidopsis thaliana ecotype Columbia (Col-0) was used as a WT plant. Testcross experiments were conducted in *gcs1/gcs1*,[18,20] RPS5Apro::tdTomato-LTI6b,[31] *kpl/kpl*,[39] *WOX2p::H2B-GFP + WOX2p::LTI-tdTomato* double marker,[40] *AGL62::GFP*[41] and WT plants. Seeds were sterilized with 5% sodium hypochlorite containing 0.5% Triton X-100 and germinated on plates containing 0.5× Murashige and Skoog salts (pH 5.7) (Wako Pure Chemical), 2% sucrose, Gamborg's B5 vitamin solution (Sigma), and 0.3% Gelrite (Wako Pure Chemical) in a growth chamber at 21.5°C under 24 h of light after cold treatment (4°C) for 2 days. Ten-day-old seedlings were transferred to Metro-Mix 350 soil (Sun Gro) and grown at 21.5°C under 24 h of light. The rice variety "Nipponbare" (*Oryza sativa* ssp. *japonica*) was used as the wild type (WT) for comparing the seed phenotype and as the source of the OEPPAP lines. Both lines were grown in a greenhouse under 13 h light/11 h dark conditions at 28 °C day/20 °C night until flowering.

METHOD DETAILS

Construction of *Atbg_ppap* mutant and *OEAtBG_ppap* lines

An *Atbg_ppap* mutant was made with CRISPR/Cas9 technology using an *AtBG_ppap*-targeting vector construct based on the pDe-Cas9 systems.[60] Gene-specific gRNA sequences unique for *AtBG_ppap* (At5g42100) were designed using tools available on the CRISPRdirect website (https://crispr.dbcls.jp/). gRNAs that contained restriction enzyme recognition sites around the Cas9 cleavage position were selected. Vector construction and generation of mutants were performed as described previously.[61] The primer sequences used for this construction are shown in Table S1. Through selections with BASTA (Fujifilm Wako) and CAPS analyses, mutants containing 1 bp deletion (Atbg_ppap-cr1) in the open reading frame of *AtBG_ppap* were isolated. An *OEAtBG_ppap* construct was prepared by combining pCAMBIA1302-derived 35S promoter (600 bp) followed by the first half of the *AtBG_ppap* sequence containing its functional domain (1134 bp), GFP encoding sequence (715 bp), remaining half of *AtBG_ppap* sequence harboring intron and second exon (575 bp), and NOS terminator. For a rescue construct, the expression of *AtBG_ppap* was driven with 1531 bp of its native promoter by cloning it and substituting it for the 35S promoter in the earlier mentioned *OEAtBG_ppap* construct.

Primers used for the preparation of constructs are shown in Table S1. The homozygous mutants of *Atbg_ppap/Atbg_ppap* were transformed with Agrobacterium harboring the construct and phenotypic changes were observed in the transgenic lines.

Construction of AtSWEET10-GFP line

The *AtSWEET10-GFP* construct was generated from a genomic clone of *AtSWEET10* (At5g50790), including a 2573-bp region 5' upstream from the initiation ATG and a 1293-bp region 3' downstream from the stop codon. GFP was fused to the *AtSWEET10* separated by a GGGGSGGGGSGGGS-linker,[62] just before the stop codon. The fluorescent protein-fusion construct was transferred to pBIN40,[59] which has been modified from pBIN19. Agrobacterium-mediated methods[63] were used to generate transgenic plants. Primers used for this experiment are listed in Table S1.

The phloem end phenotypic analyses

For staining of silique tissue, WT or other marker line flowers were emasculated at stage 12c[64] and pollinated with WT, *gcs1/gcs1*, *kpl/kpl* or *Atbg_ppap/Atbg_ppap* pollen grains. Siliques were collected at 0, 1, 2, and 3 DAP. After the samples were dissected and viewed with differential interference contrast microscopy, they were rinsed with Milli-Q (Millipore)–purified water and softened with 1 M NaOH for about 16 hours. The samples were directly stained with aniline blue solution [0.1% (w/v) aniline blue and 0.1 M K_3PO_4] for more than 3 h. Confocal/two-photon images were acquired using a laser scanning inverted microscope (LSM780-DUO-NLO, Zeiss). The images were processed using the ZEN 2010 software (Zeiss) to create maximum-intensity projection images.

CFDA and esculin

CFDA: A 100 μl drop of 5(6)-carboxyfluorescein diacetate (CFDA, optimum excitation 490 nm, emission 515 nm) (C8166, Sigma, stock solution 50 mg/ml in acetone) was applied to the cut edge of a single cotyledon at a concentration of 0.1 mg/ml in distilled water. The leaves were wrapped in plastic wrap. The fluorescence of the dyes was visualized and recorded 4 hours after the application using a White Light Laser Confocal Microscope (Leica TCS SP8 X). WT, *Atbg_ppap/Atbg_ppap* or *OEAtBG_ppap/OEAtBG_ppap* line flowers were emasculated at stage 12c[64] and pollinated with WT or *gcs1/gcs1* pollen grains. After 48 h (= 2 DAP), the stem was cut with scissors at 5 cm from the bottom of the pollinated pistil. The cut plants were placed in PCR tubes containing 100 μl CFDA solution and incubated at 22°C for 90 minutes. The ovary wall was cut off with a 27-gauge needle, and the stigma and placenta were split into two pieces. N5T medium was added dropwise to a glass bottom dish, ovules were lined up, and imaging was performed while sucking the solution. Time-lapse and Z-plane images were taken at 5-minute intervals, and 7 images were taken in 3 μm increments. Confocal images were acquired using an inverted fluorescence microscope (IX-83; Olympus) equipped with a disk scan confocal system (CSU-W1; Yokogawa Electric). Esculin: A 100 μl drop of 8 mg/ml esculin (66778-17-4, Sigma) (esculin was dissolved in distilled water with 0.2% DMSO and 0.4% absolute ethyl alcohol) was applied to the cut edge of a single cotyledon. The leaves were wrapped in plastic wrap. The fluorescence of the dyes was visualized and recorded 4 hours after the application using a White Light Laser Confocal Microscope (Leica TCS SP8 X).

Vector preparation for rice

pCAMBIA-1380 vector was used for the PPAP-overexpression (PPAP-OE) construct preparation. The 1986 bp rice UBIQUITIN promoter (pUBI) and 1275 bp long Arabidopsis-derived PPAP coding sequence were incorporated into the vector. For enhanced overexpression effect, translation enhancer (omega; 77 bp) was sandwiched between the UBI promoter and PPAP gene. For pUBI cloning, pUBI.fwd was used as forward primer and pUBI.rev was used as reverse primer. An additional set of primers, Omega.fwd as forward and Omega.rev as reverse, were used to clone the omega fragment. Infusion cloning protocol was followed to incorporate the pUBI and omega fragments amplified using the primers into the EcoRI-digested pCAMBIA-1380 vector. Next, we cloned PPAP CDS from Arabidopsis using PPAPCDS.fwd as forward and PPAPCDS.rev as reverse primers and incorporated into the earlier prepared construct by digesting it with HindIII in such a way that the CDS would be ligated between the omega sequence and NOS-terminator. Primers used for this experiment are listed in Table S1.

Rice transformation and regeneration

The method for rice transformation was conducted as previously reported.[34] For the regeneration culture, the immature embryos were transferred to a 9 cm plastic Petri Dish after co-culture. Tissues except scutellum were removed during subsequent tissue transfer using a scalpel. The divided scutella were placed faced up in a Petri Dish marked with partition on the bottom of each immature embryo. The embryos were cultured without selection at 30°C for 6 to 20 days under bright light conditions. The immature embryos may be divided by scraping off the scutellum portion with a scalpel. The 6 divided scutella were further divided into 3-5 parts using a scalpel under a stereo microscope and transferred to the selection medium. The embryos were incubated at 30°C for 7-10 days. Afterwards, the resistant callus grown from the scutellum were transferred to the redifferentiation medium. Each of the resistant calli was treated as an independent transgenic callus for each divided tissue. They were incubated for about 7 days at 30°C under light conditions and the proliferated resistant calli were transferred to redifferentiation medium. The propagated resistant calli were transferred to the re-differentiation medium. The explants were transferred to a re-differentiation medium and incubated under light conditions at 30°C for about 14 days to obtain re-differentiated shoots or regenerated young plants. The regenerated juvenile plants were directly transferred into the nursery medium. After 14 days of incubation at 30°C under light conditions, the grown plantlets were carefully separated. After carefully removing the calli, the roots were wrapped with a cotton ball and placed in a small pot in a seedling box.

The pots containing seedlings were placed on a stainless steel pad filled with 1000x Hyponex solution on a plastic rack at 25°C. After about 7 days of growth under light conditions, the pots were moved to the greenhouse.

Observation of rice pistils

Between 2-3 days after flowering, rice pistils of Nipponbare and the *osgcs1* mutant[34] were fixed in 4% paraformaldehyde, 5% acetic acid, and 50% ethanol. The pistils were vacuumed and dehydrated in an ethanol series (50%, 70% 80%, 90%, 95%, 100%) for 1 h each and then 100% ethanol overnight. These were infiltrated with 5:1, 3:1, 2:3, 1:5, 0:1 ethanol/Technovit 7100 (Kulzer, Wehrheim, Germany) for 1 h each and embedded in Technovit 7100, according to the manufacturer's instruction. These samples were cut into transverse sections (14 μm) with a rotary microtome OSK97LF506R (Ogawaseiki, Tokyo, Japan). These sections were stained for 2 h by 0.01% aniline blue (water soluble, nacalai tesque, Kyoto, Japan) in 2% K_3PO_4 (FUJIFILM Wako, Osaka, Japan) on glass slides after incubation with 2% K_3PO_4 for 30 min. The signals of aniline blue were imaged by cellSens Ver 3.0 (OLYMPUS, Sapporo, Japan) through an Olympus fluorescence microscope OLYMPUS BX51 equipped with 10x 0.40 air objective lens UPlanSApo, a filter for UV (excitation filter: 330–385 nm band pass, emission filter: 420 nm long-pass) and fitted with an Olympus DP27 camera.

Ultrastructure analyses of the amyloplasts around the final form of the phloem end *Arabidopsis thaliana* ovule samples were collected from NPT, WT, *gcs1*/*gcs1* and *Atbg_ppap*/*Atbg_ppap* at 2 DAP. The samples were fixed with 2% paraformaldehyde (PFA) and 2% glutaraldehyde (GA) in 0.05 M cacodylate buffer pH 7.4 at 4°C overnight. After this fixation, the samples were washed 3 times with 0.05 M cacodylate buffer for 30 min each and were postfixed with 2 % osmium tetroxide (OsO4) in 0.05 M cacodylate buffer at 4°C for 3 h. The samples were dehydrated in graded ethanol solutions (50%, 70%, 90%, 100%). The schedule was as follows: 50% and 70% for 30 min each at 4°C, 90% for 30 min at room temperature, and 4 changes of 100% for 30 min each at room temperature. After these dehydration processes, the samples were continuously dehydrated in 100% ethanol at room temperature overnight. The samples were infiltrated with propylene oxide (PO) 2 times for 30 min each and were put into a 70:30 mixture of PO and resin (Quetol-651; Nisshin EM Co., Tokyo, Japan) for 1 h, then kept with the tube cap open and PO was volatilized overnight. The samples were transferred to a fresh 100% resin, and were polymerized at 60°C for 48 h. The polymerized resins were ultra-thin sectioned at 80 nm with a diamond knife using an ultramicrotome (Ultracut UCT; Leica, Vienna, Austria) and the sections were mounted on copper grids. They were stained with 2% uranyl acetate at room temperature for 15 min, and then they were washed with distilled water followed by being secondary-stained with Lead stain solution (Shigma-Aldrich Co., Tokyo, Japan) at room temperature for 3 min. The grids were observed by a transmission electron microscope (JEM-1400Plus; JEOL Ltd., Tokyo, Japan) at an acceleration voltage of 100 kV. Digital images (3296 x 2472 pixels) were taken with a CCD camera (EM-14830RUBY2; JEOL Ltd., Tokyo, Japan).

QUANTIFICATION AND STATISTICAL ANALYSIS

Quantification

All the quantifications conducted are described in the main text or each Figure legend in detail.

Statistical analysis

All the statistical tests applied are specified in each Figure legend. Comparison between two groups were analyzed using Welch's t-test or Student's t-test. Comparison among more two groups were analyzed using ANOVA followed by Dunnett's multiple comparison test or Tukey's multiple comparison test.